Draft pre-print version. *The final version of this article can be found at:*
Sancho-Knapik D, Mendoza-Herrer O, Alonso-Forn D, *et al*. 2022 Vapor pressure deficit constrains transpiration and photosynthesis in holm oak: A comparison of three methods during summer drought. *Agric. For. Meteorol.* 327, 109218. https://doi.org/10.1016/j.agrformet.2022.109218

Title

Vapor pressure deficit constrains transpiration and photosynthesis in holm oak: A comparison of three methods during summer drought.

Authors

Domingo Sancho-Knapik[a,b,*], Óscar Mendoza-Herrer[a], David Alonso-Forn[a], Miguel Ángel Saz[c], Rubén Martín-Sánchez[a], José Víctor dos Santos Silva[a], Jerome Ogee[d], José Javier Peguero-Pina[a,b], Eustaquio Gil-Pelegrín[a], Juan Pedro Ferrio[a,e].

Affiliations

[a]Departamento de Sistemas Agrícolas, Forestales y Medio Ambiente, Centro de Investigación y Tecnología Agroalimentaria de Aragón (CITA), Avda. Montañana 930, 50059, Zaragoza, Spain; [b]Instituto Agroalimentario de Aragón -IA2- (CITA-Universidad de Zaragoza), Zaragoza, Spain; [c]Departamento de Geografía y Ordenación del Territorio, Universidad de Zaragoza, 50009 Zaragoza, Spain; [d]UMR 1391 ISPA, INRA, Villenave d'Ornon 33140, France; [e]Aragon Agency for research and development (ARAID), E-50018 Zaragoza, Spain.

**Correspondence author*: Tel: +34 976 716974.

E-mail address: dsancho@cita-aragon.es (D. Sancho-Knapik)

Abstract

High rates of vapor pressure deficit (VPD) can severely decrease plant productivity by reducing stomatal conductance, which might be exacerbated during Mediterranean summers due to soil water deficit. In this study, we monitored the response of holm oak, the archetype of Mediterranean trees, to changes in VPD during a summer drought period to evaluate the effects and consequences on gas exchange of the two water stresses (atmospheric and soil). Measurements were performed on trees growing in an experimental plantation over two summers with moderate drought stress by using three different methods: at the leaf level with an infrared gas analyzer, using a whole-plant chamber for short-term monitoring at the tree level, and measuring the canopy temperature for long-term monitoring. The three methods provided negative relationships between leaf conductance and VPD but with discrepancies probably associated with the measurement scale. Overall, the results showed that atmospheric and soil water stress had an additive effect. Under well-watered conditions, an increase in VPD was partially compensated by a reduction in stomatal conductance, resulting in a slight increase in the transpiration rates. With soil water deficit, the response to VPD resulted in a further decrease in stomatal conductance, reducing transpiration as a water saving strategy. The decrease in conductance in response to VPD was transitory, recovering to initial values as soon as the VPD decreased, both under well-watered and drought conditions. Due to this high sensitivity to atmospheric drought, the maximum carbon gain rates of holm oak were restricted to a short environmental window, which might modulate its physiological performance and natural distribution.

Key words

Atmospheric drought, conductance, infrared thermometry, photosynthesis, soil water deficit, whole-plant chamber.

1. Introduction

Earth's atmosphere is experiencing a global increase in dryness as a result of a rise in atmospheric evaporative demand or the so-called water vapor pressure deficit (VPD, kPa), which is projected to further increase as climate change intensifies (Jung et al., 2010; Ficklin and Novick, 2017; Dai et al., 2018; Yuan et al., 2019; Li et al., 2021). Briefly, VPD is determined by two components: i) the water vapor holding capacity of air (saturation vapor pressure), which is proportional to temperature, and ii) vapor pressure, which is the actual amount of water vapor in the atmosphere (Barkhordarian et al., 2019). This dependence on two standard climatic variables causes VPD to be a key parameter determining plant transpiration and ecosystem productivity (Seager et al., 2015; Tatarinov et al., 2015; Ficklin and Novick, 2017; López et al., 2021). High values of VPD can reduce vegetation growth (Ding et al., 2018; Yuan et al., 2019), increase forest decline (Carnicer et al., 2013; Williams et al., 2013; Restaino et al., 2016), decrease crop yields (Lobell et al., 2014), increase wildfire incidence (Williams et al., 2014; Seager et al., 2015), or affect water and carbon ecosystem cycling (McDowell and Allen, 2015). Furthermore, these negative effects are especially relevant in arid and semiarid environments such as the Mediterranean areas, as plants in this type of climate not only have to regularly cope with VPD values above 4 kPa, but also with summer droughts that promote soil water deficit during the hot season (Iglesias et al., 2007; Gil-Pelegrín et al., 2017; Peguero-Pina et al., 2020).

The mechanistic basis explaining a reduction in productivity triggered by rising VPD, either alone or in combination with soil water deficit, has been associated with photosynthetic limitations resulting from decreases in stomatal conductance (g_s) (Mediavilla and Escudero, 2003, 2004; McDowell and Allen, 2015; Grossiord et al., 2020). This ability to modify g_s with changes in VPD has also been considered the predominant form of daytime gas-exchange regulation (McAdam and Brodribb, 2016). In water-limited environments, where the difference in VPD between early morning and midday could be more than 2 kPa (Bellot et al., 2002; Barradas et al., 2004), the ability to close stomata at midday could be considered a water saving strategy to prevent excessive water loss through transpiration but at the expense of reducing carbon gain (Tatarinov et al., 2016; Peguero-Pina et al., 2020).

Different methods are being used to evaluate plant transpiration and carbon gain for a certain stress, such as the use of infrared gas analyzers (von Caemmerer and Farquhar, 1981), infrared thermometry (Jones, 1999), gravimetric methods (Peguero-Pina et al., 2018) or eddy covariance (Burba, 2013). Among these methods, the measurement of the gas exchange response of single leaves with an infrared gas analyzer (IRGA) system is one of the most common techniques used due to its simplicity and ease of handling (Alonso-Forn et al., 2021; López et al., 2021). However, it has some disadvantages. First, conditions inside the chamber generally differ from the outside; hence, to monitor plant environmental responses, measurements must be made within a few seconds after closing the leaf chamber. Even when using an IRGA system with complete environmental control inside the chamber, it is not straightforward to mimic external conditions. Second, measurements are made on a single leaf and require multiple replicates to be extrapolated to the whole canopy. These problems can be solved by using a whole-plant chamber (Liu et al., 2000; Sancho-Knapik et al., 2016) that monitors the response of the entire canopy, which could differ from the response at the leaf scale (Bonan et al., 2021). The major inconvenience of this system is its complexity when

monitoring large trees or its portability in uneasy accessible sites. Finally, another set of techniques includes the estimation of the response of plants to stress through near-surface remote sensing (Sancho-Knapik et al., 2010; Sancho-Knapik et al., 2018, and references therein). Among these other techniques, the use of infrared thermometry to monitor canopy temperature can be used for the estimation of stomatal conductance (Andrews et al., 1992; Jones, 1992; Sepulcre-Canto et al., 2007). This method is based on the decrease in leaf energy dissipation and the consequent rise in leaf temperature, triggered by the stomatal closure that occurs when plants are subjected to water stress (Jones, 1999). The method has been largely used to monitor crop fields as a possible aid for irrigation scheduling, but its main limitation is the need to measure or estimate several other environmental variables (Hipps et al., 1985). In particular, the leaf-to-air temperature difference depends not only on the cooling effect of transpiration but also on wind speed, surface roughness and net radiation (Jones, 1999).

In this study, we investigated the response of gas exchange to drought in holm oak (*Quercus ilex* L.), a key evergreen species of the Mediterranean Basin landscape. Holm oak is considered a drought-tolerant species but exhibits a water-saving strategy in response to both soil and atmospheric water stress when compared to other oaks, resulting in high stomatal control of water losses, as evidenced at hourly to seasonal scales (Tenhunen et al. 1981; Acherar & Rambal 1992; Mediavilla and Escudero, 2003; 2004; Aguadé et al. 2015; del Castillo et al. 2016; Peguero-Pina et al., 2020; Alonso-Forn et al. 2021). However, little is known about the short-term dynamics of stomatal response to atmospheric water stress, particularly with the interaction with soil water stress. Taking this into account, we hypothesized that the response to VPD of holm oak in terms of stomatal conductance would be modulated by soil water conditions. Under well-watered conditions, the stomatal conductance of holm oak would be transiently reduced under atmospheric water stress, counteracting the increase in transpiration with higher VPD. Conversely, under soil water deficit conditions, the stomatal conductance (already limited by soil drought) would be comparatively less sensitive to VPD. As a consequence of the stomatal closure, we also hypothesized that atmospheric drought by itself would contribute negatively to the overall carbon balance of holm oak. For this purpose, we monitored *Q. ilex* (holm oak) trees growing in an experimental plantation (where trees receive irrigation and maintenance) over two summers with moderate drought stress by using the three methods proposed above: gas exchange at the leaf level (leaf cuvette), gas exchange at the tree level measured with a whole-plant chamber, and canopy infrared thermometry. Three main objectives were: (1) to compare and evaluate the three methods for monitoring plant responses to changes in VPD; (2) to evaluate the interaction of soil and atmospheric water stress on stomatal conductance and transpiration of *Q. ilex*; and (3) to study the consequences of both stresses on carbon gain.

2. Materials and Methods

2.1 Experimental conditions and plant material

The study took place in an experimental field plot located at CITA de Aragón (41.723° N, 0.809° W, Zaragoza, Spain) during the summers of 2018 and 2019 under Mediterranean climatic conditions (mean annual temperature 15.4 °C, total annual precipitation 298 mm; see annual climate patterns in Fig. S1). The experimental plot is a holm oak plantation first destined for truffle production, where the total soil depth is ca. 60 cm. Trees of *Quercus ilex* subsp. *rotundifolia* from this plot were 25 years old and

planted in 1998 using a pattern of 6x6 m. Trees were maintained in good health conditions, were irrigated with sprinklers (35-40 L m^{-2}) every week from April to September, and were pruned every two years during winter to obtain trees with homogeneous rounded-shape canopies. The tree height was ca. 3 m, the diameter of the orthogonal projection of the tree canopy ranged between 2.0 and 2.5 m, and the percentage of canopy cover on the soil surface was ca. 14%. Twice a year (during early winter and early summer), the experimental plot is cleaned mechanically, eliminating the presence of the herbaceous and shrubby stratum.

In both summers, irrigation was stopped in mid-June (prior to the monitoring) to allow drought conditions to develop. During the following weeks, plant monitoring took place at the tree level (using the plant chamber) in 2018, and at the leaf level (with the leaf cuvette) and canopy level (with the infrared thermometry) in 2019. No differences in the summer climatic patterns between 2018 and 2019 were noticed (Fig. S1). Furthermore, the same range in VPD and soil water conditions were evaluated.

Two soil water statuses were considered during the experiments: well-watered and soil water deficit conditions. The water potential threshold between them was set at -0.5 MPa, as from this value, *Q. ilex* subsp. *rotundifolia* starts to close stomata, according to Alonso-Forn et al. (2021). Thus, soil under well-watered conditions referred to trees growing with a plant water potential at predawn (Ψ_{pd}) or soil water potential (SWP) between 0 and -0.5 MPa, while soil water deficit conditions (or soil water stressed conditions) were those at a Ψ_{pd} or SWP between -0.5 and -2.0 MPa. Trees experienced these moderate soil water deficit conditions during ca. 3 weeks in both the 2018 and 2019 summers.

2.2 Gas exchange measurements at the leaf level

Gas exchange measurements at the leaf level were conducted periodically during the summer of 2019 (from the beginning of July to mid-August) with an open gas exchange system (CIRAS-3, PP-Systems, Amesbury, MA, USA) fitted with an automatic universal leaf cuvette (PLC6-U, PP-Systems, Amesbury, MA, USA). At the end of the experiment, we obtained a total of 12 measurement days: 6 days during well-watered conditions and another 6 during soil water deficit conditions. Measurements were performed in the morning (between 7:30 and 10:00 h solar time) and at midday (between 11:00 and 14:00 h) on sun-exposed, fully developed, current-year attached leaves located in the southern exposure of the lower canopy (ca. 1.30 m above ground). Three to five leaves were randomly selected and measured from each of the 3 specimens of *Q. ilex* subsp. *rotundifolia* used for infrared monitoring (see Section 2.4). The sample size for each day of measurement ranged from 18 to 30 leaves (3 to 5 leaves x 2 times x 3 trees). The controlled cuvette CO_2 concentration was 400 μmol mol^{-1} and the saturating photosynthetic photon flux density was 1500 μmol m^{-2} s^{-1}. The VPD inside the leaf cuvette was set to coincide with the atmospheric value. It should be noted that setting VPD values lower than 1.5 and higher than 3.5 KPa, required several minutes and were not always reached. Prior to the gas-exchange measurements, plant water potential was measured at predawn (Ψ_{pd}) with a Scholander pressure chamber following the methodological procedure described by Turner (1988).

2.3 Gas exchange measurements at the whole-plant level

Measurements at the whole-plant level were performed in 2018 using one whole-plant chamber (described below) to monitor, one after other, 6 different specimens of *Q. ilex*. First, just after stopping the irrigation (mid-June), we monitored 4 trees under well-watered conditions in the following two weeks. Then, three weeks later (toward the end of July), 2 other trees under soil water deficit conditions were monitored. Each tree monitoring lasted 24 h. As a result, we monitored 6 trees x 24 h. Plant water potential at predawn (Ψ_{pd}) was measured the day before each tree monitoring in shoots of holm oak with a Scholander pressure chamber. The photosynthetic active radiation (PAR) was also registered with a quantum sensor QSO (Apogee Instruments, Logan, USA).

The whole-plant chamber (Fig. S2) consisted of a Teflon fluorinated ethylene propylene copolymer (FEP) film rolled and stapled into an aluminum cylindrical frame (diameter, d = 200 cm; height, h = 180 cm) ending in an open top cone (base d = 200 cm, h = 100 cm; open hole d = 50 cm). Teflon FEP was used because of its slow permeability to liquids and gasses and its excellent transmission (between 90 and 95%) in the infrared and visible range of the solar spectrum (Liu et al., 2000). For easier installation and portability, the chamber was built as two halves that were screwed together on a PVC base (220 x 220 cm). To accommodate the trunk and the air inlet tubes, we made 3 circular holes in the base: one in the middle (d = 20 cm) for the trunk and two others (d = 15 cm) facing opposite corners, one for each air inlet tube. The base was also cut in half through the trunk hole opening so that it could be moved on and off the tree. A sleeve of sealed-cell foam was placed around the trunk, enabling the chamber base to compress the sleeve and form a tight seal around the stem. This design separated the tree from the soil to eliminate the effects of soil and root respiration on CO_2 determinations (Miller et al., 1996). Finally, the joining between the chamber and the base was also sealed with plastic adhesive tape to ensure maximum impermeability.

The air-supply system consisted of a semiradial tube air fan (TD-1300/250 Silent Ecowatt, Soler & Palau, Spain) with an output of 20 m^3/min attached to an aluminum tube (d = 25 cm) that collected air from 4 m above the ground. The output side of the fan was attached to another aluminum tube (d = 25 cm) that was split with a "T" connector into two smaller aluminum tubes (d = 15 cm), each one going through each hole of the base into the chamber. Each of these tubes ended in a 1 m aluminum tube (d = 15 cm), placed horizontally on the base inside the chamber, and upper perforated with small holes (d_{hole} = 0.5 cm) for a better diffusion of the incoming air into the chamber (Fig. S2).

To monitor the tree, we simultaneously measured the CO_2 concentration and H_2O vapor in the air prior to entering the chamber and just before the open top exit using an infrared gas analyzer (CIRAS-3 DC, PP-Systems, Amesbury, MA, USA). Measurements were recorded every 5 minutes. Additionally, we calculated VPD inside the chamber by measuring air temperature and relative humidity using a Hobo Pro RH/Temp data logger (Onset Computer Bourne, MA, USA) located 1 m above the base. The VPD inside the chamber was used for further evaluation of the plant response and for statistical analysis.

We calculated tree transpiration (E, mol H_2O s^{-1} $tree^{-1}$) and total conductance (g_t, mol H_2O s^{-1} $tree^{-1}$) using the following equations (von Caemmerer and Farquhar, 1981):

$$E = \frac{W \times (e_{out} - e_{in})}{(P - e_{out})} \quad \text{Eq. (1)}$$

$$g_t = \frac{E \times (P - \frac{e_{leaf} + e_{out}}{2})}{(e_{leaf} - e_{out})} \quad \text{Eq. (2)}$$

where W is the mass flow of air entering the chamber (mol H_2O s^{-1}), e_{in} is the partial pressure of water vapor of reference air supplied to the cuvette (mbar), e_{out} is the partial pressure of water vapor in the air inside the chamber (mbar), P is the atmospheric pressure (mbar), and e_{leaf} is the saturated water vapor pressure inside the leaf (mbar). After obtaining g_t, we removed most of the values of g_t coinciding with values of VPD below 0.5 kPa as they had high uncertainty and resulted in aberrant values. We also calculated the net photosynthesis (A_N, μmol CO_2 s^{-1} $tree^{-1}$; von Caemmerer and Farquhar, 1981) as $A_N = (C_{in} \times W) - [C_{out} \times (W + E)]$ Eq. (3), where C_{in} and C_{out} are the CO_2 concentrations of air entering and exiting the chamber, respectively. Finally, water use efficiency (WUE, μmol CO_2 mol^{-1} H_2O) and intrinsic water use efficiency (iWUE, μmol CO_2 mol^{-1} H_2O) were calculated as WUE = A_N/E and iWUE = A_N/g_t, respectively.

2.4 Canopy infrared thermometry

Infrared (IR) thermometry was used to monitor three holm oak trees during 49 consecutive summer days, from the 20th of June 2019 (with well-watered soil conditions) to the 8th of August 2019 (with soil water deficit conditions). The canopy temperature of each individual was measured with infrared thermometers (IRT 757-500, TC Ltd, Uxbridge, U.K.), custom-calibrated against a 4-wire platinum resistance thermometer (PT100) over the range 5-50 °C in a high-precision water bath (Julabo FP50, Julabo GmbH, Seelbach, Germany). IR thermometer sensors were located ca. 3.5 m height from the ground, pointing down to the south-side of the upper canopy, at an angle of 45° and at a distance of 2 m from the target to cover 1 m^2 of the canopy surface. Air temperature, horizontal wind speed and photosynthetic active radiation (PAR) were recorded, with a 4-wire PT100 probe, a cup anemometer (Oche Control y Equipamientos S.L., Cadrete, Spain) and a quantum sensor QSO (Apogee Instruments, Logan, USA), respectively. Data from the aforementioned sensors were recorded every 30 seconds with a CR1000 datalogger (Campbell Scientifics, Logan, USA). Additionally, relative humidity was registered every 10 minutes with three Hobo Pro RH/Temp data loggers (U23-001; Onset Computer Corp., Pocasset, MA, USA). Soil water potential (SWP) was recorded every 2 minutes using 3 soil water potential sensors connected to a data logger (Teros 21/Em50, METER Group, Inc., Pullman, WA, USA) and installed below each tree canopy at a distance of 50 cm from each trunk and at 30 cm below ground, representative of the root system. Atmospheric pressure was retrieved from a meteorological station located 17 km SW from the site (Zaragoza Airport, 41° 39' 38" N; 1° 0' 15" W, 249 m.a.s.l.).

For calculations, all data were integrated at 30-minute intervals. We calculated VPD by combining temperature records from PT100, which was found to be the most reliable, and atmospheric vapor pressure, calculated from the relative humidity records. Canopy temperature depression (CTD) was calculated as the difference between air temperature and canopy temperature. CTD is positive when the canopy is cooler than the air and negative when the canopy temperature is higher than the air temperature (i.e., canopy heating), which might occur when trees reduce or stop transpiration. Leaf transpiration (E, mol H_2O m^{-2} s^{-1}) was estimated from the difference between measured canopy temperature (T_c) and modeled leaf temperature for a dry surface (T_{dry}, modeled as in Barbour et al. 2000), following the next energy balance equation (Jones, 1992):

$$E = C_{\mathrm{p}}(g_{\mathrm{bH}} + g_{\mathrm{r}})(T_{\mathrm{dry}} - T_{\mathrm{c}})/L \quad \text{Eq. (4)}$$

where C_p is the molar specific heat constant of air at constant pressure (29.2 J mol^{-1} K^{-1}), g_{bH} and g_r are the boundary layer (sensible) heat conductance and radiative heat conductance, respectively (in m^2 s^{-1} mol^{-1}), and L is the molar heat of vaporization (44012 J mol^{-1}). For a more detailed explanation of the calculation of E using infrared thermometry, see Section 6 (Appendices A and B). The total leaf conductance (g_t, mol H_2O m^{-2} s^{-1}) was then calculated according to von Caemmerer and Farquhar (1981) using Eq. (2).

2.5 Statistical analysis

To compare conductance measurements obtained with the three different methods, each single value of conductance (g^i) was standardized as $(g^i - g_{min})100/(g_{max}\text{-}g_{min})$, where g_{min} and g_{max} are the minimum and maximum conductance values, respectively, measured with well-watered soil conditions and PAR>500 μmol m^{-2} s^{-1}. Then, eventual differences across methods and water conditions in the relationship between VPD and standardized conductance were first explored with an analysis of variance (ANOVA) based on a linear model including 'method' (single leaf, plant chamber, IR thermometry), 'water' (wet, dry), log-transformed values of VPD ('logVPD'), and their interactions (built-in R functions 'lm' and 'anova'). We used log-transformed values and linear regression models as the simplest approach for testing differences in the observed (non-linear) responses. Alternative models, e.g. using untransformed variables or alternative distributions did not improve the normality of residuals, and lead to similar results (data not shown).

Nonlinear regressions between VPD and g (both measured and standardized values) were fitted using the function 'drm' from the package drc 3.0-1 (Ritz et al., 2015). After testing alternative dose-response models (e.g. exponential decay, logistic, log-logistic), we identified the log-logistic function with four parameters (self-starter function 'LL.4' in 'drm') as the function best describing the expected response across all data combinations. The advantage of using this function is that we obtained estimates of biologically meaningful parameters, which could be directly compared. In particular, for LL.4, these parameters were the slope (VPD vs. g), the upper and lower limits of g, and the effective dose 50 (ED50, namely the VPD causing a 50% reduction in g).

To characterize connections among environmental and plant variables and determine their relative importance in controlling leaf conductance, we used the IR canopy dataset to conduct a path analysis (Li, 1975). This analysis uses a path structure that consists of variables of interest with potential connectivity among the variables where the connections are based on previously well-established knowledge. Based on the variables and the connections, a set of multiple linear regression models is constructed, and the partial regression coefficients are defined as path values that indicate the causative power of each connection (Kimm et al., 2020). Structural equation models for the path analysis were fitted using the function 'sem' from package Lavaan 0.6-10 (Rosseel, 2012) and represented with the function 'semPath' (package semPlot 1.1.2; Epskamp, 2015). The model included atmospheric water vapor pressure (Vp), photosynthetic active radiation (PAR) and soil water potential (SWP) as exogenous variables, and air temperature (Tair, as a function of PAR), atmospheric vapor pressure deficit (VPD, as a function of Tair and Vp), total conductance (g_t, as a function of VPD, PAR and SWP), and transpiration (E, as a function of g_t and VPD) as endogenous variables. To account

for temporal variations in environmental drivers, path analyses were performed considering data during the entire daytime (from 6:00 to 18:00 h solar time), data from only the morning (from 6:00 to 10:00 h), data from only the midday (from 10:00 to 14:00 h), and data from only the afternoon (from 14:00 to 18:00 h).

3. Results

3.1 Time course of transpiration and stomatal conductance

The monitoring of gas exchange at the leaf level showed that during well-watered conditions (predawn water potential, Ψ_{pd}>-0.5 MPa), an increase in VPD from 2 to 4 kPa between the morning and midday entailed a reduction in stomatal conductance (g_s) from 0.35 to 0.15 mol H_2O m^{-2} s^{-1} with hardly any variation in leaf transpiration (E, Fig. 1). Under water deficit conditions (-0.5>Ψ_{pd}>-2.0 MPa), the measured values of g_s and E decreased (Fig. 1). Moreover, increases in VPD smaller than 1 kPa between the morning and midday entailed reductions in g_s from ca. 0.15 to close to zero mol H_2O m^{-2} s^{-1} and reductions in E from ca. 3 to 1 mmol H_2O m^{-2} s^{-1} (Fig. 1).

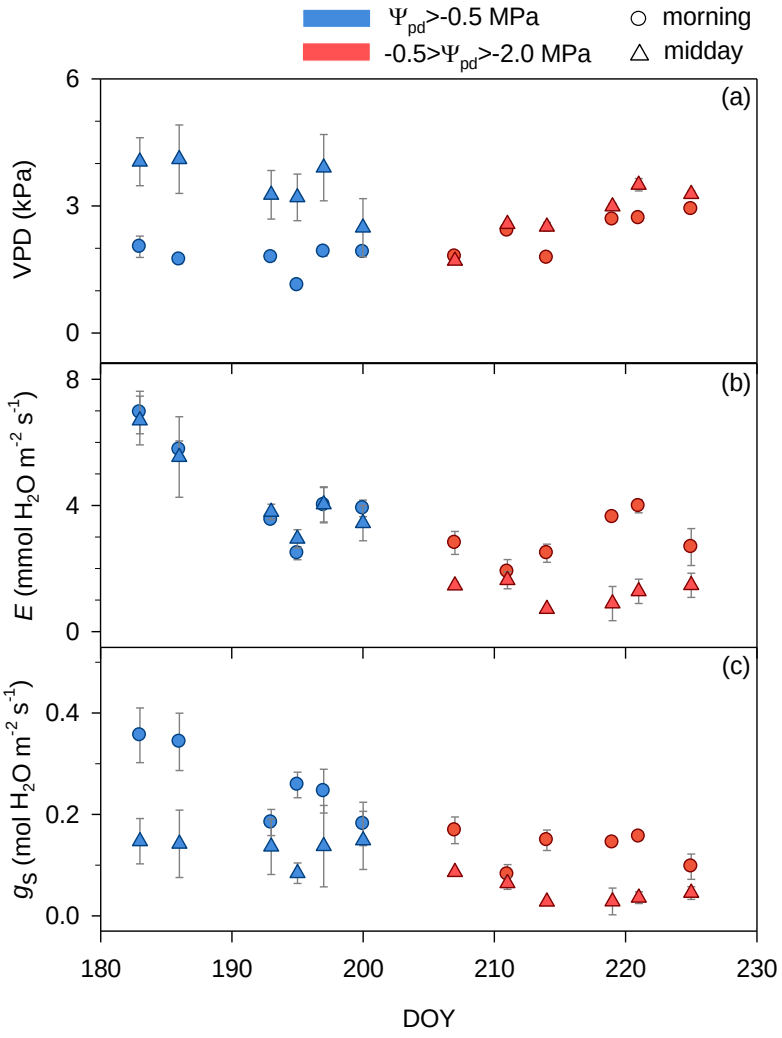

Fig. 1 Example of gas exchange monitoring at leaf level of one specimen of *Quercus ilex* subsp. *rotundifolia*. (a) Vapor pressure deficit (VPD), (b) transpiration (E), (c) stomatal conductance (g_s). Data are mean±se (n = 3 to 5 leaves). Blue shapes correspond to well-watered

conditions (predawn water potential, Ψ_{pd}>-0.5MPa), while red shapes correspond to water deficit conditions (-0.5>Ψ_{pd}>-2.0MPa). Circles and triangles are measurements made in the morning (8:00 to 10:00 solar time) and midday (11:00 to 14:00), respectively.

The monitoring of *Q. ilex* with the whole-plant chamber was carried out on days with a VPD and air temperature inside the chamber that exceeded 4 kPa (Fig. 2a) and 35 °C, respectively, during some point of the day. It should be noted that when comparing the conditions inside the chamber against the external conditions, we noticed a significant warming effect of the air inside the chamber, especially important during the afternoon (from 13:00 to 18:00 h solar time), but without reaching extreme temperatures (Table S1). Considering the experimental conditions inside the chamber, well-watered trees (with a Ψ_{pd}>- 0.5 MPa) showed transpiration rates (*E*) of approximately 0.02 mol H_2O s^{-1} $tree^{-1}$, which remained nearly constant between 7:30 and 16:00 h solar time, concurring with a photosynthetically active radiation (PAR) higher than 500 μmol m^{-2} s^{-1}. Out of this frame of time, PAR seemed to be the limiting factor, as *E* decreased sharply to zero with the reduction in PAR (Figs. 2b, S3). Notably, despite the sharp increase in VPD (from ca. 3 to 5 kPa), we found only a slight increase in E during the afternoon. In contrast, the total conductance (g_t) for well-watered trees decreased during the day from maximum values recorded in the early morning (ca. 7:30 h solar time; Fig. 2c). Concerning the water-stressed trees (with a Ψ_{pd} between -0.5 and -2 MPa), we clearly recorded lower values of *E* and g_t than for well-watered trees (Fig. 2). Moreover, *E* in drought stressed trees did not remain constant, showing a maximum value of ca. 0.010 mol H_2O s^{-1} $tree^{-1}$ at 10:00 h with a VPD=2 kPa, which decreased to 0.005 mol H_2O s^{-1} $tree^{-1}$ for an increase in VPD toward 5 kPa (Figs. 2a,b). In addition, g_t in water-stressed trees also decreased as in well-watered trees, experiencing a strong reduction from early morning to midday and remaining nearly constant during the afternoon until PAR=500 μmol m^{-2} s^{-1} (Fig. 2c).

Draft pre-print version. *The final version of this article can be found at:*
Sancho-Knapik D, Mendoza-Herrer O, Alonso-Forn D, *et al*. 2022 Vapor pressure deficit constrains transpiration and photosynthesis in holm oak: A comparison of three methods during summer drought. *Agric. For. Meteorol.* 327, 109218. https://doi.org/10.1016/j.agrformet.2022.109218

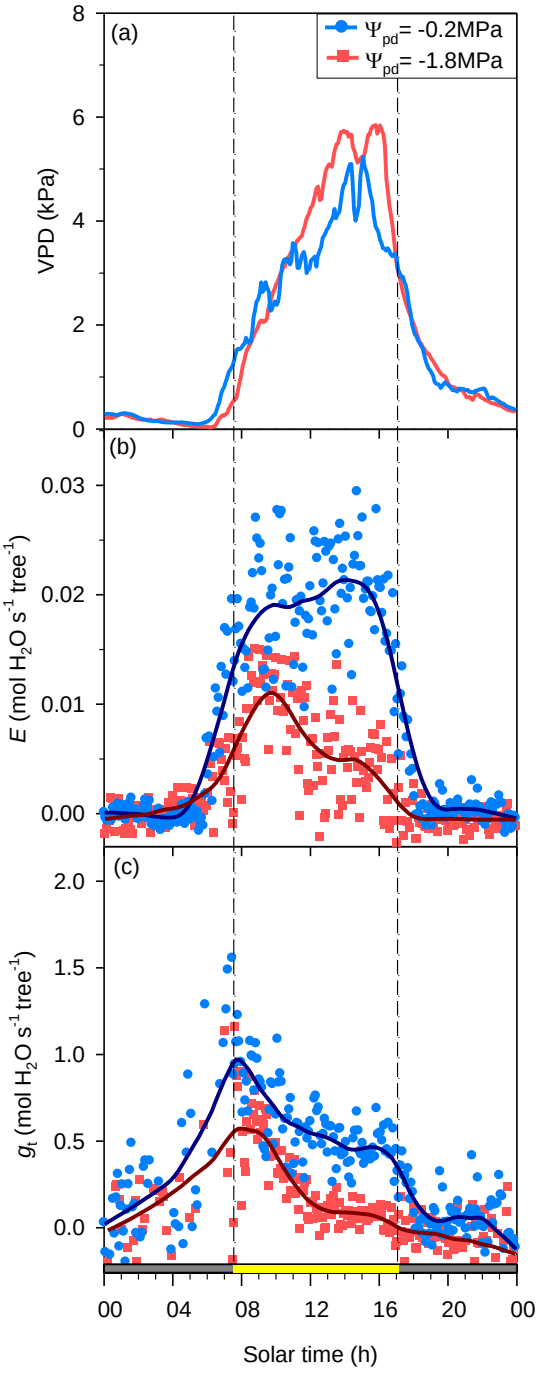

Fig. 2 Examples of one day monitoring of two different trees of *Quercus ilex* subsp. *rotundifolia* using a whole-plant chamber. (a) Vapor pressure deficit (VPD), (b) plant transpiration (*E*), (c) total conductance (g_t). Lines are a smoothing of the data points. Blue lines and circles correspond to one well-watered tree (predawn water potential, Ψ_{pd}=-0.2MPa) measured at mid-June, while red lines and squares correspond to one water stressed tree (Ψ_{pd}=-1.8MPa) measured at the end of July. Yellow and grey bars on the x-axis correspond to periods with a photosynthetic active radiation higher and lower than 500 µmol m^{-2} s^{-1}, respectively. Dashed lines define this radiation interval period through the graphs.

The use of infrared thermometry to monitor holm oak canopies during the summer showed that canopy temperature depression (CTD) varied throughout the day and with drought progression. During the day, the lowest values of CTD were usually recorded at midday (12 h solar time; Fig. S4), whereas the highest values were generally recorded during the afternoon (15-18 h solar time; Fig. S4), coinciding with the maximum values of VPD (Fig. 3a). However, it should be noted that on some days, especially those under soil water deficit conditions, the CTD values during the afternoon were lower than those during the early morning (6-9 h solar time); therefore, the maximum CTD values on those days were found during the early morning (Figs. 3b, S4). Over the season, CTD varied in accordance with changes in SWP (Fig. S4). At the beginning of the monitored period (DOY 170-190, 'well-watered' phase), SWP remained close to zero, and CTD remained positive most of the time (i.e., air temperature was consistently higher than the canopy temperature, Fig. S5). This was followed by a sharp decline in SWP from DOY 190 to 210 ('soil drying' phase), remaining under steadily low SWP from DOY 210 to 220 ('drought' phase). As the soil dried and the SWP became more negative, the negative values of CTD (occurring when the air temperature was lower than the canopy temperature, Fig. S5) became more frequent (Fig. S4). For example, when the SWP was -0.9 MPa, CTD remained negative at midday, reaching values up to -3 ^{o}C (Fig. 3b).

Maximum values of *E* estimated with the IR method were recorded every day after midday, concurring with the maximum values of VPD (Fig. 3c). At the beginning of the experiment, under well-watered soil conditions, trees showed maximum values of *E* between 5 and 8 mmol H_2O m^{-2} s^{-1}. As the SWP became more negative, the maximum values of *E* progressively decreased to a range between 3 and 5 mmol H_2O m^{-2} s^{-1} (Fig. 3c). Concerning total conductance (g_t), we surprisingly observed maximum values of g_t around dawn (ca. 4:30 to 5:30 h, with PAR<500 μmol m^{-2} s^{-1}), probably due to the low values of VPD measured at that time of the day (between 0.5 and 1.0 KPa; Fig. 3) which increases the estimation error of the method. Apart from that, g_t estimated with IR when PAR was higher than 500 μmol m^{-2} s^{-1} followed a similar pattern to g_t monitored with the whole-plant chamber, with high values generally recorded in the early morning (7:30 h solar time) that decreased as the day went by (Fig. 2d). As long as the soil became drier, the values of g_t reached lower values throughout the entire day (Fig. 3d). It should be noted that Fig. 3 also highlights three consecutive days (indicated with arrows) with different values of g_t obtained at midday (84, 123, and 160 mmol H_2O m^{-2} s^{-1}), associated with three different levels of VPD (6.5, 4.4, and 3.2 kPa, respectively) and air temperature (41, 37 and 33 °C, respectively) recorded at the same time, showing an increase in g_t in accordance with a decrease in VPD.

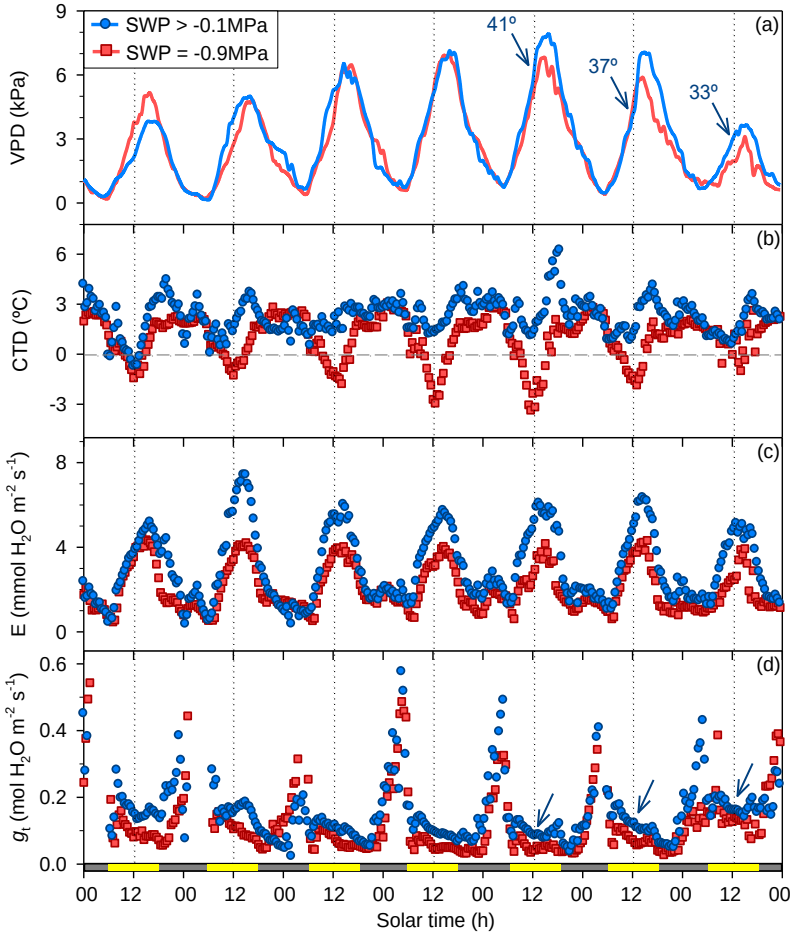

Fig. 3 Monitoring of *Quercus ilex* subsp. *rotundifolia* using the canopy infrared thermometry method during two heatwaves differing in soil water conditions. (a) Vapor pressure deficit (VPD), (b) canopy temperature depression (CTD), (c) plant transpiration (*E*), (d) total conductance (g_t). Blue lines and circles correspond to a 7-day period (day of the year 176 to 182) of one well-watered tree (soil water potential, SWP>-0.1 MPa, Fig. S4), while red lines and squares correspond to another 7-day period (day of the year 201 to 207) of the same tree under soil water deficit conditions (SWP=-0.9 MPa, Fig. S4). Yellow and grey bars on the x-axis correspond to periods with a photosynthetic active radiation higher and lower than 500 μmol m^{-2} s^{-1}, respectively. Blue arrows indicate three consecutive days differing in VPD and g_t recorded at noon for well-watered conditions; air temperatures associated to each moment are indicated above arrows in (a).

3.2 Response of stomatal conductance to VPD and soil water deficit.

The exploratory ANOVA that assessed the general response of stomatal conductance (standardized *g*) to log-transformed VPD showed significant differences between monitoring methods and water conditions and complex interactions (Table S2). In particular, the intercept term using the leaf chamber was significantly lower than that using the other two methods (P=0.036), whereas the (negative) slope in response to VPD was significantly steeper using the IR method (P=0.040). As expected, the intercept term was higher in well-watered plants (P<0.001), but the slope in response to VPD was more negative (P<0.001). In addition to these general patterns, the highly significant interaction

terms ('method:water', P=0.002; 'method:water:logVPD', P<0.001) indicated that both the intercept and the slope differed for each 'method x water' combination.

When VPD was related to plant conductance (considering only those values with VPD>0.5 kPa and PAR>500 μmol m^{-2} s^{-1}), we found consistent relationships for the three methods used (Fig. 4). For well-watered trees, an increase in VPD from 1 to 5 kPa induced a reduction in stomatal conductance (g_s) measured with the leaf cuvette method from ca. 0.35 to 0.05 mol H_2O m^{-2} s^{-1} (Fig. 4a). The same increase in VPD also resulted in a decrease in g_t measured with the other two methods: from ca. 0.95 to 0.28 mol H_2O s^{-1} $tree^{-1}$ measured with the whole-plant chamber and from 0.38 to 0.15 mol H_2O m^{-2} s^{-1} for the IR thermometry (Figs. 4a,b). For soil water deficit conditions, the values of conductance obtained with the three methods were lower than those under well-watered conditions for every single value of VPD (Fig. 4). When conductance was standardized by means of the maximum and minimum values recorded for well-watered conditions, the adjusted equations of the three different methods shared similar values, although with slightly different patterns (Fig. 4d, Table 1). The IR thermometry method and the single leaf method under drought showed a quasi-exponential shape, with a progressive decline in conductance, starting from relatively low VPD values (Fig. 4d, see also Fig. 4a,c). Conversely, a plateau in conductance until VPD ≈ 2 kPa, followed by a steeper decline, was evident for the plant chamber method, as well as for the single leaf method under well-watered conditions (Fig. 4d, see also Fig. 4a,b). The parameters estimated for the log-logistic curves (Table 1) confirmed that ED50 (i.e., the value of VPD at which conductance dropped by half) was in the range of 1-3 kPa, regardless of the method and water conditions. Considering the parameter uncertainty, the highest estimates for ED50 (2.5-3.0 kPa) and slope (6.1-6.2% kPa-1) were found for the plant chamber method, being significantly higher than for the IR thermometry (ED50= 1.4-1.7 kPa; slope= 1.8-3.0% kPa-1). Conversely, we did not find significant differences in ED50 and slope between well-watered and drought conditions. Only for the plant chamber method were the estimated upper and lower limits (indicative of maximum and minimum conductance) significantly higher in well-watered than in drought conditions. For the single leaf method, the uncertainties were generally large, particularly under drought conditions, thus preventing a proper statistical comparison, but still the most significant estimates were in range with the other methods.

		Watered conditions (Ψ>-0.5 MPa)		Drought conditions (-0.5>Ψ>-2.0 MPa)	
		Estimate (95% confidence interval)	P-value	Estimate (95% confidence interval)	P-value
Single leaf	Slope	6.7 (2.3, 11.1)^{ab}	**0.003**	7.3 (-1.2, 15.7)^{a}	0.090
	Lower Limit	13.8 (4.1, 23.4)^{a}	**0.005**	14.6 (11.1, 18.1)^{a}	**<0.001**
	Upper Limit	66.8 (56.7, 76.9)^{a}	**<0.001**	481 (-6202, 7165)^{ab}	0.886
	ED50	2.4 (2.1, 2.6)^{ab}	**<0.001**	1.1 (-1.5, 3.7)^{ab}	0.412
Plant chamber	Slope	6.1 (4.5, 7.6)^{a}	**<0.001**	6.2 (2.4, 10)^{a}	**0.001**
	Lower Limit*	16.2 (13.4, 19)^{a}	**<0.001**	1.8 (-4.1, 7.7)^{b}	0.542
	Upper Limit*	67.4 (63.7, 71.1)^{a}	**<0.001**	35.4 (30.4, 40.5)^{a}	**<0.001**
	ED50	2.5 (2.4, 2.6)^{a}	**<0.001**	3 (2.7, 3.4)^{b}	**<0.001**
	Slope	1.8 (0.9, 2.6)^{b}	**<0.001**	3 (1.9, 4)^{a}	**<0.001**

Draft pre-print version. *The final version of this article can be found at:*
Sancho-Knapik D, Mendoza-Herrer O, Alonso-Forn D, *et al.* 2022 Vapor pressure deficit constrains transpiration and photosynthesis in holm oak: A comparison of three methods during summer drought. *Agric. For. Meteorol.* 327, 109218. https://doi.org/10.1016/j.agrformet.2022.109218

IR thermometry	Lower Limit	4.9 (-5.1, 14.7)[a]	0.341	5 (1, 9)[b]	**0.015**
	Upper Limit	92.9 (62, 123.8)[a]	**<0.001**	74.3 (52.5, 96.6)[b]	**<0.001**
	ED50	1.7 (1.2, 2.3)[b]	**<0.001**	1.4 (1.1, 1.7)[a]	**<0.001**

Table 1 Parameter estimates of the log-logistic curves describing the relationship between vapor pressure deficit (VPD) and standardized conductance (as shown in Fig. 4d) for the different methods and water conditions. Ψ refers to either predawn water potential (single leaf and plant chamber) or soil water potential (IR thermometry). In bold *P*-values < 0.05. Parameters differing significantly (i.e. with non-overlapping confidence intervals) are indicated with asterisks (between soil water conditions) and letters (across methods).

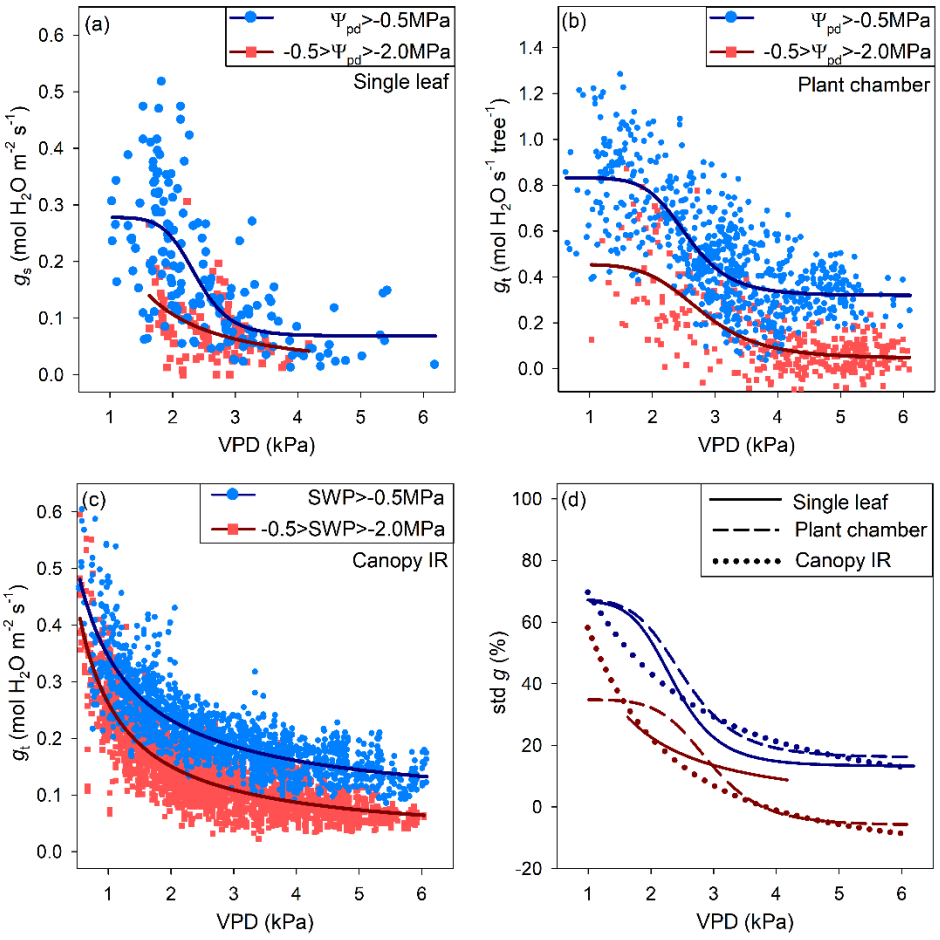

Fig. 4 Relationship between vapor pressure deficit (VPD) and stomatal conductance (g_s) or total conductance (g_t) for *Quercus ilex* subsp. *rotundifolia* using: (a) a single leaf cuvette (*n*=3 trees, 12 measurement days), (b) a whole-plant chamber (for well-watered conditions, *n*=4 trees, 1 measurement day each tree; for water deficit conditions, *n*=2 trees, 1 day each tree,), and (c) the canopy infrared (IR) thermometry (*n*=3 trees, 49 days). The relationship between VPD and standardized leaf conductance (std *g*) for the three methods is shown in (d). Blue lines and circles correspond to well-watered conditions (predawn water potential, Ψ_{pd} or soil water potential SWP>-0.5 MPa), while red lines and squares correspond to soil water deficit conditions (-0.5>Ψ_{pd} or SWP>-2.0 MPa).

A closer look at the response over time during three heatwaves (associated with high VPD) showed that the response to VPD was transient and very dynamic, regardless

of prevailing soil water conditions (Fig. 5). The first event (DOY from 176 to 183), under well-watered conditions (circles/solid lines; Fig. 5), showed a nearly linear decline and recovery in g_t. However, this decline in the mean daytime g_t was not enough to compensate for the increase in VPD, and the mean daytime E increased from ca. 3.5 to 4.5 mmol m^{-2} s^{-1}. In the second event (DOY=199-207), during the soil drying phase (diamonds/dashed lines; Fig. 5), the increase in VPD coincided with a progressive decline in SWP, resulting in a sharper decrease in g_t and a slight decrease in E. Nevertheless, after the high-VPD event, the values of g_t recovered to values similar to the pre-event values. Finally, during the steady drought phase (DOY=219-224; squares/dotted lines), we found a weaker decline in g_t, which resulted in nearly constant E. Notably, post-event g_t values (white square; Fig. 5) were even larger than pre-event g_t (black square), although this could be attributed to the rather cloudy conditions before the event (only 6.4 hours with PAR>500 µmol m^{-2} s^{-1}, against 9-10 hours in the following days), which may have caused a slight light limitation.

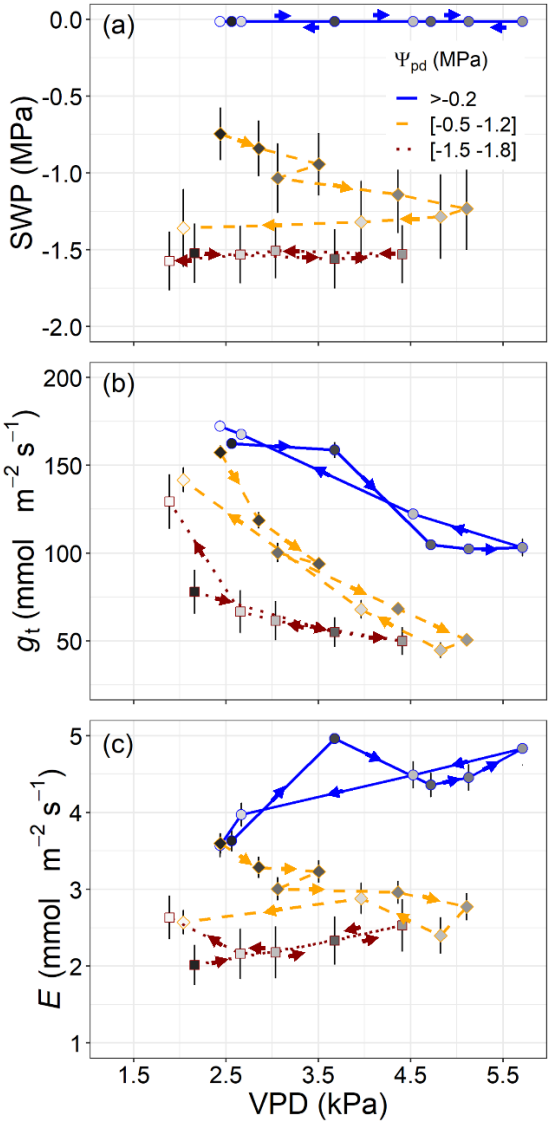

Fig. 5 Evolution of daytime average (PAR>500 µmol m^{-2} s^{-1}) of soil water potential (SWP), IR thermometry-derived total conductance (g_t) and transpiration (E) during three heatwaves (associated to VPD>4 kPa). Arrows and gray intensity indicate the timing within each high-VPD

event, with black and white values corresponding to pre-event and post-event conditions, respectively (VPD<= 2.5 kPa). Error bars indicate the standard error of the mean, integrating daily and inter-tree variability through error propagation. Circles / solid lines, diamonds / dashed lines, and squares / dotted lines, denote the three events, occurring during the well-watered (days of the year, DOY: 176-183), soil drying (DOY: 199-207) and drought (DOY: 219-224) phases shown in Fig. S4. As a reference we include in the legend the predawn water potential (Ψ_{pd}) values during each event.

3.3 Response of photosynthesis and water use efficiency to VPD and soil water deficit

A reduction in net photosynthesis (A_N) throughout the day associated with increases in VPD was recorded with the whole-plant method in both well-watered and water-stressed trees (Figs. 6a,b). This reduction in A_N for well-watered trees started at a VPD value of ca. 2.5 kPa, the value from which we started to record values of A_N close to zero for water-stressed trees (Fig. 6b). Concerning the water use efficiency, Fig. 6c shows a decrease in this parameter with increasing VPD. Similarly, the intrinsic water use efficiency in drought-stressed trees slightly decreased with increases in VPD (Fig. 6d). However, the intrinsic water use efficiency in well-watered trees remained constant for most of the VPD values, even though an increase from 1 to 2 kPa was detected.

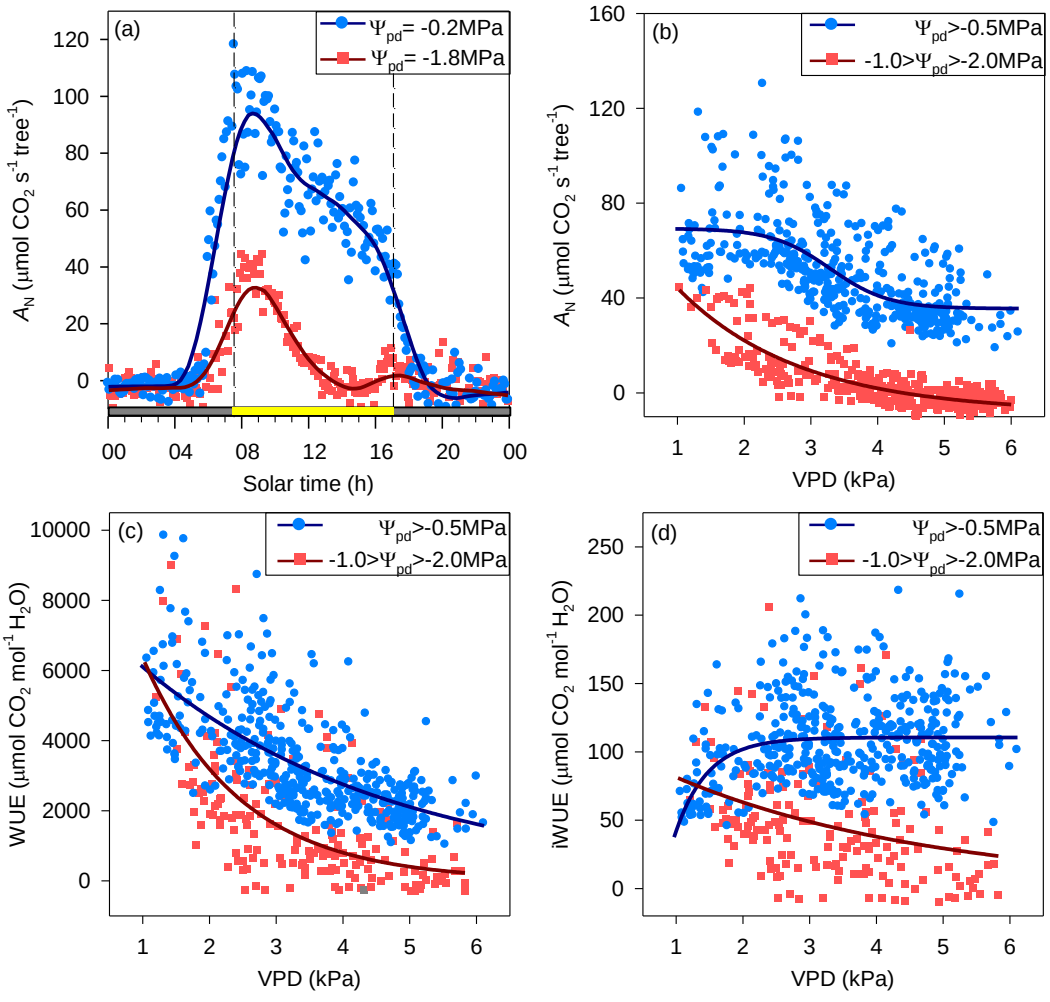

Fig. 6 Evolution of net photosynthesis (A_N) throughout the day, monitored with a whole-plant chamber on one holm oak under well-watered conditions (blue; predawn water potential, Ψ_{pd}=-0.2MPa) and on other specimen under drought conditions (red; Ψ_{pd}=-1.8 MPa) (a). Relationship between vapor pressure deficit (VPD) and: A_N (b), water use efficiency (WUE) (c) and intrinsic water use efficiency (iWUE) (d). Blue lines and circles in (b), (c) and (d) correspond to two holm oaks under well-watered conditions (Ψ_{pd}>-0.5 MPa), while red lines and squares correspond to two other holm oaks under water stressed conditions (-0.5>Ψ_{pd}>-2.0 MPa). Yellow and grey bars in (a) correspond to periods with a photosynthetic active radiation higher and lower than 500 μmol m^{-2} s^{-1}, respectively.

3.4 Factors regulating the response to VPD and soil water deficit

The path analysis showed that both SWP and VPD had a similar effect on g_t when considering the daytime (Fig. 7). However, the effect of VPD on g_t was slightly higher than the effect of SWP during the morning and afternoon, while it was slightly lower during midday (Fig. 7). We only found a weak effect of PAR on g_t during the morning and afternoon, coinciding with the periods with partially light-limited conditions. As expected, both VPD and g_t contributed to *E*, but with variable proportions during the day, increasing the relative weight of g_t from morning to afternoon (Fig. 7). With regard to the link between the different environmental drivers, variations in VPD were largely driven by *T*air, with a minor contribution of variations in *V*p, particularly during the morning. In turn, variations in *T*air during the morning were strongly coupled to the rise in PAR, but this association was weak during midday, when PAR was nearly constant, and in the afternoon, when *T*air declined much more slowly than PAR. The three exogenous variables in the model (*V*p, PAR and SWP) were independent, showing no clear associations among them.

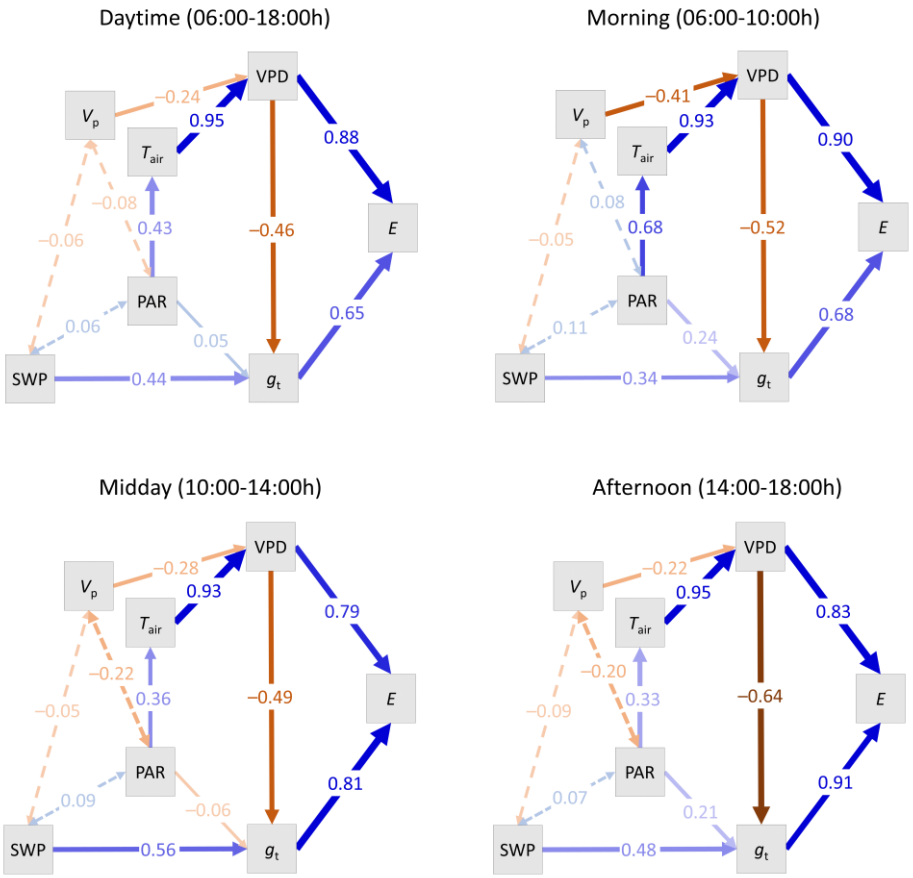

Fig. 7 Path analysis considering infrared data from the daytime and from each period of the daytime (morning, midday and afternoon). VPD, atmospheric vapor pressure deficit; SWP, soil water potential; g_t, total conductance; *E* transpiration; T_{air}, air temperature; V_p, atmospheric water vapor pressure; PAR, photosynthetic active radiation. Blue are positive correlations and red are negative ones. Line thickness is proportional to the standardized parameter estimation (also shown in numerical labels). Bi-directional dashed lines indicate associations between exogenous variables (*V*p, PAR and SWP). Uni-directional solid lines indicate the 'causal' associations included in the structural model.

4. Discussion

4.1 Evaluating methods to monitor plant response to VPD

In general, total leaf conductance was negatively related to rising VPD, but the variability at the local level of VPD was different across the three methods used (single leaf cuvette, whole-plant chamber and canopy IR thermometry), mainly due to the different measurement scale. The total leaf conductance obtained with IR thermometry decreased exponentially for the whole range of VPD evaluated, while the total leaf conductance obtained with the whole-plant chamber remained constant for VPD values lower than 2 kPa and higher than 4 kPa, mainly decreasing from 2 to 4 kPa (Fig. 3). This discrepancy could be explained by the different portions of the canopy measured by each method (Jones, 1992; Rey-Sánchez et al., 2016). On the one hand, the IR method monitored the southern exposure of the upper canopy, i.e., the area with the highest evaporative demand during the day and, therefore, the area potentially most sensitive to changes in VPD. On the other hand, the response given by the whole-plant chamber

resulted from the sum of the different parts of the tree, where the response of the southern exposure parts might be smoothed with the response of the northern and lower-canopy areas (Tenhunen et al., 1990; Bonan et al., 2021). Concerning the single leaf cuvette, the variation in stomatal conductance to changes in VPD resulted in an intermediate response between the two other methods. This might also be due to the location of the leaves measured with this technique, which was the southern exposure of the lower canopy, which might have a lower evaporative demand than the southern upper canopy, but still higher than the northern exposure.

Regarding a procedural comparison between methods, each of them has some advantages and some other disadvantages, taking into account their complexity, invasiveness and degree of assumption. First, the leaf cuvette easily allows the measurement of any single leaf due to its portability but hardly allows continuous monitoring due to its highest invasiveness. In fact, setting VPD values lower than 1.5 and higher than 3.5 KPa, required several minutes and not always were reached. This resulted in few measured values at high VPD, notably during soil water deficit conditions where we were not able to obtain measurements at VPD values higher than 4.5 kPa. In any case, the trend of the regression shown in Fig. 4a for soil water deficit conditions indicates that values of VPD>4.5 kPa might yield values of g_s close to the minimum conductance.

Second, the whole-plant chamber can monitor the response of the entire tree with a minimum assumption but with the highest methodological complexity. In this study, we gave conductance units for this method by tree instead of by m^2, taking into account that absolute values were not comparable with values obtained from the other methods. Alternatively, the total leaf area of the tree could be estimated by using different models and assumptions, such as the estimation from the transmittance of the sun beam (Lang and Murtrie, 1992) or using a terrestrial laser scanner (Hu et al., 2018). Another issue to highlight when using the whole-plant chamber is the significant warming effect found during the afternoon, which increased VPD in comparison to the external conditions. This limits the duration of the monitoring campaigns and should be taken into account when upscaling the results at the plantation level.

Finally, the IR technique registers the response of a certain area of the canopy, allowing noninvasive measurements without modifying the microclimatic conditions surrounding the tree. However, using the IR method requires a higher degree of assumption, for example, the estimation of the incident radiation reaching the leaf surface (Appendix B), the wind speed input, or the calculation of the boundary layer conductance (see Appendix A for details). In addition, to obtain conductance values from the estimated transpiration by IR, the uncertainty of the method increases with lower values of VPD, which implies values close to zero in the denominator of Eq. A6. In fact, at VPD values lower than 1 kPa (found around dawn), the estimated stomatal conductance may result in excessively large and erratic values.

In summary, all three methods have advantages and disadvantages, providing similar relationships between leaf conductance and drought stress but with peculiarities that complement each other (Fig. 8).

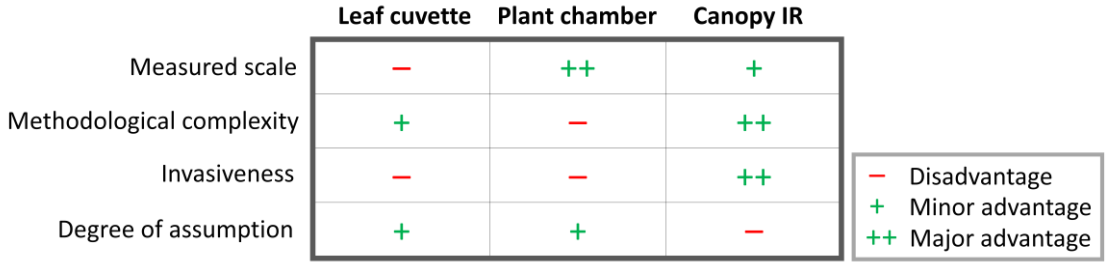

Fig. 8 Summary of the main advantages and disadvantages of the three methods tested in this study. –: disadvantage; +: minor advantage; ++: major advantage.

4.2 Effect of VPD and soil water deficit on Q. ilex

In well-watered trees of *Q. ilex* subsp. *rotundifolia*, an increase in VPD was compensated by a reduction in stomatal conductance, as previously reported in the same species (Mediavilla and Escudero, 2004; Aguadé et al., 2015). In our study, an increase from 2 to 4 kPa resulted in a reduction of ca. 25% in conductance, independent of soil conditions (Fig. 3d). When an increase in VPD to 4 kPa was combined with soil water deficit, the response of *Q. ilex* to both stresses resulted in a further ca. 20% decrease in stomatal conductance. Thus, soil and atmospheric water stress have an additive effect, with soil drying causing a general decline in *g* but not affecting the critical threshold in response to VPD (ca. 2 kPa; see ED50 in Table 1). Consequently, an analogous response of *g* to VPD is maintained regardless of soil water conditions, rejecting our first hypothesis.

Overall, our results confirm that VPD is a substantial regulator of the stomatal response and, hence, transpiration (Novick et al., 2016, 2019; Grossiord et al., 2020). However, under well-watered conditions, the reduction in *g* only partially compensated for the increase in transpiration with VPD at both the hourly and daily scales. In this regard, the water-saving response of *Q. ilex* in front of VPD was less effective than in more isohydric Mediterranean species (Tatarinov et al., 2015). Conversely, under soil water deficit conditions, the combined effect of atmospheric and soil water stress entailed in *Q. ilex* a decrease in water loss by the further reduction in stomatal conductance. This could be an effective strategy to reduce transpiration-driven xylem tension and prevent drought-induced embolism (Martin-St Paul et al., 2017; Peguero-Pina et al., 2018; Taylor et al., 2020). Moreover, this water-saving strategy together with the high xylem resistance to drought-induced cavitation shown by *Q. ilex* subsp. *rotundifolia* both, in stems (water potential at which 50% of hydraulic conductivity is lost, P50, ca. -6.0 MPa) and shoots (P50 ca. -6.5 MPa; Alonso-Forn et al., 2021), entails a wide safety margin for avoiding runaway embolism (Vilagrosa et al., 2003). Additionally, it is worth considering the different performance that *Q. ilex* might have in populations from France or Italy, where the other subspecies, *Q. ilex* subsp. *ilex* showed a similar sensitivity to VPD and soil water deficit but with a lower tolerance to xylem tension (Tognetti et al., 1998) and therefore a lower safety margin. The existence of different ecotypes within this paradigm of Mediterranean trees (Peguero-Pina et al., 2014) must be taken into account in terms of their ecological interpretation.

The path analysis showed that, overall, soil dryness and evaporative demand are both important to explain stomatal closure, but their relative weight varies over the day.

During the morning, SWP had the lowest effect on g_t, partly due to the more favorable environmental conditions (lower VPD) and the role of light limitations during this period. At midday, when light is not limiting and VPD still does not reach its daily maximum, SWP shows the largest effect on g_t. Finally, during the afternoon, coinciding with the largest evaporative demand, VPD shows the strongest effect on g_t. This implies that the afternoon decline in stomatal conductance due to elevated VPD still plays a major role under well-watered conditions and, as discussed below, becomes critical for photosynthesis, even under moderate drought stress, as in our study. In terms of water balance, however, the water-saving strategy is successful, allowing nearly constant transpiration rates to be maintained during the day under well-watered conditions and even declining under drought (Alonso-Forn et al., 2021).

4.3 Consequences of higher VPD on carbon gain

Holm oak is highly sensitive to drought, as demonstrated in this study and in previous ones (Mediavilla and Escudero, 2003, 2004; Aguadé et al., 2015; Sancho-Knapik et al., 2018; Alonso-Forn et al., 2021). This fact restricts the maximum productivity of holm oak (measured as carbon gain) to a narrow window of environmental conditions, i.e., VPD<2 kPa and SWP>-0.5 MPa, in our experiment usually registered for well-watered trees during only two hours per day on average, from ca. 7:30 to 9:30 h solar time (Fig. 5). Additionally, regardless of VPD, values of leaf temperature above 30 °C might also induce a reduction in the maximum photosynthetic rates (Gratani et al., 2000) due to limitations in the metabolism (Haldimann et al., 2008), which might contribute to a reduction in WUE. Therefore, the real carbon gain of holm oak can be much lower than its potential, becoming less efficient using water resources, which may threaten the long-term productivity, growth, and survival of this species, in accordance with our second hypothesis.

In practice, when evaluating the summer environmental conditions recorded during IR monitoring (i.e., from the 20th of June to the 8th of August 2019), we found that only the 14.7% of daylight hours with PAR>500 μmol m^{-2} s^{-1} are prone to achieve the maximum carbon gain rates. However, as an evergreen tree, *Q. ilex* could also gain carbon during the rest of the vegetative period (from March to November; Corcuera et al., 2005; Alonso-Forn et al., 2022) where the window for optimal conditions might be larger (Fig. S1) and thus compensate for the summer Mediterranean season. This has implications not only for ecosystem productivity but also for the management of tree orchards. Holm oak is used in plantations for truffle production, where the soil water deficit is eliminated with well-designed irrigation schedules (Águeda et al., 2010). If this had been our case and the irrigation had not been stopped, maintaining well-watered conditions during all the experiment, the percentage of hours holm oak would have achieved maximum photosynthesis rates would have only increased to 29.6% of the total daylight hours. Therefore, atmospheric water stress may still prevent full optimal conditions despite eliminating the soil water deficit. This suggest that irrigation schedules that keep soils at field capacity could be unnecessary and a waste of water if VPD already limits the maximum photosynthesis rates.

Given the importance of VPD in determining the carbon gains of holm oak, one would expect that the natural distribution of this species would also be dependent on the range of VPD values throughout the vegetative period. Effectively, when analyzing the natural distribution of holm oak in a northeast region of Spain (Fig. S6), we noticed that

the natural distribution of holm oak practically coincides with the areas with lower VPD during the vegetative period (from March to November), suggesting a relevant role of VPD in shaping vegetation similar to other factors such as soil properties or rainfall geographic patterns.

5. Conclusion

The methods used in this study to monitor VPD complement each other, with the whole-plant chamber providing an overall view of the response of the entire tree and the IR thermometry providing monitoring throughout the complete summer drought period in a noninvasive way. When compared to the single leaf measurements, the three methods provided similar relationships between VPD and conductance with discrepancies associated with the measurement scale. The results showed that atmospheric and soil water stress had an additive effect. Under well-watered conditions, an increase in VPD was partially compensated by a reduction in stomatal conductance, resulting in a slight increase in the transpiration rates. With soil water deficit, the response to VPD resulted in a further decrease in stomatal conductance, reducing transpiration as a water saving strategy. Finally, this high sensitivity to drought restricts the maximum carbon gain rates of holm oak to particular environmental conditions that might modulate its physiological performance and natural distribution.

6. Appendices

6.1 Appendix A. Calculation of leaf conductance using the infrared thermometry method

Leaf transpiration (E, in mol m^{-2} s^{-1}) was estimated from the difference between measured canopy temperature (T_c), and modelled leaf temperature for a dry surface (T_{dry}), according to energy balance equations (Jones, 1992):

$$E = C_p(g_{bH} + g_r)(T_{dry} - T_c)/L \qquad \text{Eq. (A.1)}$$

where C_p is the molar specific heat constant of air at constant pressure (29.2 J mol^{-1} K^{-1}), g_{bH} and g_r are boundary layer (sensible) heat conductance and radiative heat conductance, respectively (in m^2 s^{-1} mol^{-1}), and L is the molar heat of vaporization (44012 J mol^{-1}). G_{bH} and g_r were calculated following Ball et al. (1988) and Jones (1992), respectively:

$$g_{bH} = 1/(3.8LA^{1/4}u^{-1/2}) \qquad \text{Eq. (A.2)}$$

$$g_r = (4\sigma\varepsilon_l T_{air}^2)/C_p \qquad \text{Eq. (A.3)}$$

where LA is the average individual leaf area (in m^2), u is wind speed (in m s^{-1}), σ is the Stefan-Boltzmann constant ($5.67*10^{-8}$ W m^{-2} K^{-4}), and ε_l is long-wave emissivity of the leaf (0.98). T_{dry} was estimated using the leaf temperature model described in Barbour et al. (2000), after removing the evaporative term ($L*D$, where D is the water vapor concentration deficit (mol mol^{-1})):

$$T_{dry} = \frac{(g_{bH}+g_r)(Q_0*r_t)}{C_p(r_t+(sL/C_pP)(g_{bH}+g_r))} + T_{air} \qquad \text{Eq. (A.4)}$$

where Q_0 is the isothermal net radiation (in W m^{-2}, for calculations see Appendix B), r_t is total leaf resistance to water vapor (stomatal + boundary layer, in m^2 s^{-1} mol^{-1}), s is the slope of the curve relating temperature to saturated vapor pressure (in kPa K^{-1}), and P is the pressure in kPa. The slope s was calculated following (Postl and Bolhàr-Nordenkampf, 1983; Barbour et al., 2000):

$$s = \mathrm{a}\{\frac{[(T_{air}+\mathrm{b})(\mathrm{c}-2\frac{T_{air}}{\mathrm{d}})-T_{air}(c-\frac{T_{air}}{d})]}{(T_{air}+b)^2}\} * exp\{T_{air}[\frac{(c-\frac{T_{air}}{d})}{(T_{air}+b)}]\} \quad \text{Eq. (A.5)}$$

where a=6.13753, b=255.57, c=18.564 and d=254.4.

Total leaf conductance (g_t, in mol m^{-2} s^{-1}) was calculated according to von Caemmerer and Farquhar (1981):

$$g_t = E\,\frac{[1-(wi+wa)/2]}{(wi-wa)} \quad \text{Eq. (A.6)}$$

where w_i and w_a stand for the mol fractions of water vapor inside the leaf and in the surrounding air, respectively. Total leaf resistance (r_t=1/g_t) was used as an input variable in Eq. A4, hence calculations were made iteratively, setting an initial value for g_t=0.2 mol m^{-2} s^{-1}, and recalculating with equations A.1-A.6 until the input and output values converged to a mean absolute difference <0.0001 mol m^{-2} s^{-1}.

6.2 Appendix B. Calculation of isothermal net radiation

Horizontal radiation (Q_{sensor}) was determined from local measurements of photosynthetically active radiation (PAR) (quantum sensor QSO, Apogee Instruments, Logan, USA), assuming a typical ratio of shortwave radiation to PAR of 0.5 MJ mol^{-1} (Jones, 1992). We estimated the fraction of diffuse radiation (K_{diff}) from the transmitted fraction (K_t), according to Boland et al. (2008):

$$K_{diff} = 1/[1 + \exp\,(8.6K_t - 5)] \quad \text{Eq. (B.1)}$$

where K_t is calculated as the ratio between measured horizontal radiation and theoretical maximum horizontal solar radiation, as determined from the solar constant (1370 W m^{-2}) and solar elevation (for details see Appendix 7 in Jones, 1992). From K_{diff}, we calculated diffuse (Q_{diff}) and direct (Q_{dir}) radiation reaching the sensor. Following Lambert's cosine law, we determined incident direct radiation in the canopy surface ($Q_{dir\text{-}canopy}$) multiplying Q_{dir} by the ratio between the cosine of the angle between the surface and the sun (cos ξ), for the canopy and the sensor, respectively (Jones, 1992):

$$\cos\xi = [(\sin\lambda\cos h)(-\cos\alpha\sin\chi) - \sin h\,(\sin\alpha\sin\chi) + (\cos\lambda\cos h)\cos\chi]\cos\delta + [\cos\lambda\,(\cos\alpha\sin\chi) + \sin\lambda\cos\chi]\sin\delta \quad \text{Eq. (B.2)}$$

where λ is the latitude, h is the hour angle of the sun, α and χ are the zenith angle and azimuth of the surface, respectively, and δ is declination. Δ and h were determined using the functions *declination* and *hourangle*, available in the *R* package *insol* 1.2. For the sensor, χ=0 (horizontal surface) and α becomes irrelevant. For the canopy, χ= 45° and α=189.2°. Finally, total isothermal net radiation (Q_0) reaching the canopy was calculated as the sum of Q_{diff} and $Q_{dir\text{-}canopy}$, multiplied by an average leaf absorption coefficient of 0.5 (Jones, 1992), and a light harvesting efficiency, which accounts for self-shading within the canopy, of 0.62 in *Q. ilex* (Esteso-Martínez et al. 2006).

Declaration of Competing Interest

The authors declare that they have no known competing financial interests or personal relationships that could have appeared to influence the work reported in this paper.

Funding

This work was supported by MCIN/AEI/10.13039/501100011033 [grant number PID2019-106701RR-I00]; Gobierno de Aragón-Fondo de Inversiones de Teruel (FITE) and Gobierno de España [grant project FITE-2017-PETRA]; and by Gobierno de Aragón [research group H09_20R]. Work of D.A-F. was supported by FPI-INIA [grant number BES-2017-081208]; work of J.V.S.S. was supported by MCIN/AEI [grant number PRE2020-094944]; and work of R.M-S. was supported by Gobierno de Aragón.

Supplementary material

Supplementary material associated with this article can be found at the end of the manuscript.

References

Acherar, M., Rambal, S. 1992. Comparative water relations of four Mediterranean oak species. Vegetatio 99–100, 177–184. https://doi.org/10.1007/BF00118224

Aguadé, D., Poyatos, R., Rosas, T., Martínez-Vilalta, J., 2015. Comparative drought responses of *Quercus ilex* L. and *Pinus sylvestris* L. in a montane forest undergoing a vegetation shift. Forests 6, 2505-2529. https://doi.org/10.3390/f608250510.3390/f6082505

Águeda, B., Fernández-Toirán, L.M., de Miguel, A.M., Martínez-Peña, F. 2010. Ectomycorrhizal status of a mature productive black truffle plantation. For. Syst. 19(1), 89-97. https://doi.org/10.5424/fs/2010191-01170

Alonso-Forn, D., Peguero-Pina, J.J., Ferrio, J.P., Mencuccini, M., Mendoza-Herrer, Ó., Sancho-Knapik, D., Gil-Pelegrín, E., 2021. Contrasting functional strategies following severe drought in two Mediterranean oaks with different leaf habit: *Quercus faginea* and *Quercus ilex* subsp. *rotundifolia*. Tree Physiol. 41, 371–387. https://doi.org/10.1093/treephys/tpaa135doi:10.1093/treephys/tpaa135

Alonso-Forn, D., Peguero-Pina, J.J., Ferrio, J.P., García-Plazaola, J.I., Martín-Sánchez, R., Niinemets, U., Sancho-Knapik, D., Gil-Pelegrín, E. 2022. Cell-level anatomy explains leaf age-dependent declines in mesophyll conductance and photosynthetic capacity in the evergreen Mediterranean oak *Quercus ilex* subsp. *rotundifolia*. Tree Physiol. Tpac049. https://doi.org/10.1093/treephys/tpac049

Andrews, P.K., Chalmers, D.J., Moremong, M., 1992. Canopy-air temperature differences and soil water as predictors of water stress of apple trees grown in a humid, temperate climate. J. Amer. Soc. Hort. Sci. 117(3), 453-458. https://doi.org/10.21273/JASHS.117.3.453

Ball, M.C., Cowan, I.R., Farquhar, G.D., 1988. Maintenance of leaf temperature and the optimization of carbon gain in relation to water loss in a tropical mangrove forest. Aust. J. Plant Physiol. 15, 263-276. https://doi.org/10.1071/PP988026310.1071/pp9880263.

Barbour, M.M., Fischer, R.A., Sayre, K.D., Farquhar, G.D., 2000. Oxygen isotope ratio of leaf and grain material correlates with stomatal conductance and grain yield in irrigated wheat. Aust. J. Plant Physiol., 27, 625–637. https://doi.org/10.1071/PP99041 doi:10.1071/pp99041.

Barkhordarian, A., Saatchi, S.S., Behrangi, A., Loikith, P.C., Mechoso, C.R., 2019. A recent systematic increase in vapor pressure deficit over tropical South America. Sci. Rep. 9, 15331. https://doi.org/10.1038/s41598-019-51857-8.

Barradas, V.L., Ramos-Vázquez, A., Orozco-Segovia, A., 2004. Stomatal conductance in a tropical xerophilous shrubland at a lava substratum. Int. J. Biometeorol. 48(3), 119-27. https://doi.org/10.1007/s00484-003-0195-x doi: 10.1007/s00484-003-0195-x

Bellot, J., Urbina, A.O., Bonet, A., Sanchez-Montahud, J.R. 2002. The effects of treeshelter on the growth of *Quercus coccifera* L. seedlings in semiarid environment. Forestry 75(1), 89. https://doi.org/10.1093/forestry/75.1.89

Bonan, G.B., Patton, E.G., Finnigan, J.J., Baldocchi, D.D., Harman, I.N. 2021. Moving beyond the incorrect but useful paradigm: reevaluating big-leaf and multilayer plant canopies to model biosphere-atmosphere fluxes – a review. Agric. For. Meteorol. 306, 108435. https://doi.org/10.1016/j.agrformet.2021.108435

Boland, J., Ridley, B., Brown, B. 2008. Models of diffuse solar radiation. Renew. Energy 33, 575-584. https://doi.org/10.1016/j.renene.2007.04.012

Burba, G., 2013. Eddy covariance method for scientific, industrial, agricultural, and regulatory applications: a field book on measuring ecosystem gas exchange and areal emission rates. LI-COR Biosciences, Lincoln, NE, USA, 331 pp.

Carnicer, J., Barbeta, A., Sperlich, D., Coll, M., Peñuelas, J., 2013. Contrasting trait syndromes in angiosperms and conifers are associated with different responses of tree growth to temperature on a large scale. Front. Plant Sci. 4, 409. https://doi.org/10.3389/fpls.2013.00409

Corcuera, L., Morales. F., Abadía, A., Gil-Pelegrín, E. (2005) Seasonal changes in photosynthesis and photoprotection in a *Quercus ilex* subsp. *ballota* woodland located in it supper altitudinal extreme in the Iberian peninsula. Tree Physiol. 25:599–608. https://doi.org/10.1093/treephys/25.5.599

Dai, A., Zhao, T., Chen, J., 2018. Climate change and drought: A precipitation and evaporation perspective. Curr. Clim. Change Rep. 4(3), 301–312. https://doi.org/10.1007/s40641-018-0101-6

Ding, J., Yang, T., Zhao, Y., Liu, D., Wang, X., Yao, Y., Peng, S., Wang, T., Piao, S., 2018. Increasingly important role of atmospheric aridity on Tibetan alpine grasslands. Geophys. Res. Lett. 45, 2852–2859. https://doi.org/10.1002/2017GL076803

Epskamp, S., 2015. semPlot: Unified visualizations of structural equation models. Struct. Equ. Model. 22(3), 474–483. https://doi.org/10.1080/10705511.2014.937847

Esteso-Martínez, J., Valladares, F., Camarero, J.J., Gil-Pelegrín, E., 2006. Crown architecture and leaf habit are associated with intrinsically different light-harvesting efficiencies in *Quercus* seedlings from contrasting environments. Ann. For. Sci. 63, 511-518. http://dx.doi.org/10.1051/forest:200603310.1051/forest:2006033.

Ficklin, D.L., Novick, K.A., 2017. Historic and projected changes in vapor pressure deficit suggest a continental-scale drying of the United States atmosphere. J. Geophys. Res. Atmos. 122(4), 2061–2079. https://doi.org/10.1002/2016jd025855

Gil-Pelegrín, E., Saz, M.A., Cuadrat, J.M., Peguero-Pina, J.J., Sancho-Knapik, D., 2017. Oaks under 26editerranean-type climates: functional response to summer aridity. In: Gil-Pelegrín, E., Peguero-Pina, J.J., Sancho-Knapik, D., eds. Oaks physiological ecology. Exploring the functional diversity of genus *Quercus* L. Cham, Switzerland: Springer International, 137–193.

Gratani, L., Pesoli, P., Crescente, M.F., Aichner, K., Larcher, W. 2000. Photosynthesis as a temperature indicator in *Quercus ilex* L. Global Planet. Change 24, 153–163. https://doi.org/10.1016/S0921-8181(99)00061-2

Grossiord, C., Buckley, T.N., Cernusak, L.A., Novick, K.A., Poulter, B., Siegwolf, R. T.W., Sperry, J.S., McDowell, N.G., 2020. Plant responses to rising vapor pressure deficit. New Phytol. 226(6), 1550–1566. https://doi.org/10.1111/nph.16485

Haldimann, P., Gallé, A., Feller, U. 2008. Impact of an exceptionally hot dry summer on photosynthetic traits in oak (*Quercus pubescens*) leaves. Tree Physiol. 28, 785–795. https://doi.org/10.1093/treephys/28.5.785

Hipps, L.E., Ashrar, G., Kanemasu, E.T., 1985. A theoretically based normalization of environmental effects on foliage temperature. Agric. Forest Meteorol. 35, 113-122. https://doi.org/10.1016/0168-1923 (85)90078-4

Hu, R., Bournez, E., Cheng, S., Jiang, H., Nerry, F., Landes, T., Saudreau, M., Kastendeuch, P., Najjar, G., Colin, J., Yan, G. 2018. Estimating the leaf area of an individual tree in urban areas using terrestrial laser scanner and path length distribution model. ISPRS J. Photogramm. Remote Sens. 144, 357–368. https://doi.org/10.1016/j.isprsjprs.2018.07.015

Iglesias, A., Garrote, L., Flores, F., Moneo, M., 2007. Challenges to manage the risk of water scarcity and climate change in the Mediterranean. Water Resour. Manag. 21, 775–788. https://doi.org/10.1007/s11269-006-9111-6

Jones, H. G., 1992. Plants and Microclimate; Cambridge University Press: Cambridge, U.K.; Vol. 2nd. Ed. ISBN 9780511845727.

Jones, H.G., 1999. Use of infrared thermometry for estimation of stomatal conductance as a possible aid to irrigation scheduling. Agric. Forest Meteorol. 95, 139-149. https://doi.org/10.1016/S0168-1923 (99)00030-1

Jung, M., Reichstein, M., Ciais, P., Seneviratne, S. I., Sheffield, J., Goulden, M. L., Bonan, G., Cescatti, A., Chen, J., de Jeu, R., Dolman, A.J., Eugster, W., Gerten, D., Gianelle, D., Gobron, N., Heinke, J., Kimball, J., Law, B.E., Montagnani, L., Zhang, K.E., 2010. Recent decline in the global land evapotranspiration trend due to limited moisture supply. Nature 467(7318), 951–954. https://doi.org/10.1038/nature09396

Kimm, H., Guan, K., Gentine P., Wu J., Bernacchi C.J., Sulman, B.N., Griffis T.J., Link C., 2020. Redefining droughts for the U.S. Corn Belt: The dominant role of atmospheric vapor pressure deficit over soil moisture in regulating stomatal behavior of Maize and Soybean. Agric. Forest Meteorol. 287, 107930. https://doi.org/10.1016/j.agrformet.2020.107930

Lang, A.R.G., McMurtriebm R.E. 1992. Total leaf areas of single trees of Eucalyptus grandis estimated from transmittances of the sun's beam. Agric. Forest Meteorol. 58:79-92. https://doi.org/10.1016/0168-1923(92)90112-H

Li, C.C., 1975. Path Analysis – a primer. Pacific Grove. The Boxwood Press, California.

Li, M., Yao, J., Guana, J., Zhenga, J. 2021. Observed changes in vapor pressure deficit suggest a systematic drying of the atmosphere in Xinjiang of China. Atmos. Res. 248, 105199. https://doi.org/10.1016/j.atmosres.2020.105199

Liu, L., Hoogenboom, G., Ingram, K.T., 2000. Controlled-environment sunlit plant growth chambers. Crit. Rev. Plant. Sci. 19, 347–375. https://doi.org/10.1080/07352680091139268doi: 10.1080/07352680091139268

Lobell, D.B., Roberts, M.J., Schlenker, W., Braun, N., Little, B.B., Rejesus, R.M., Hammer, G.L., 2014. Greater sensitivity to drought accompanies maize yield increase in the U.S. Midwest. Science 344, 516–519. https://doi.org/10.1126/science.1251423

López, J., Way, D.A., Sadok, W., 2021. Systemic effects of rising atmospheric vapor pressure deficit on plant physiology and productivity. Glob. Change Biol. 27, 1704-1720. https://doi.org/10.1111/gcb.15548

Martin-StPaul, N., Delzon, S., Cochard, H., 2017. Plant resistance to drought depends on timely stomatal closure. Ecol. Lett. 20, 1437–1447. https://doi.org/10.1111/ele.12851

McAdam, S.A., Brodribb, T.J., 2015. The evolution of mechanisms driving the stomatal response to vapor pressure deficit. Plant Physiol. 167, 833–843. https://doi.org/10.1104/pp.114.252940

McAdam, S.A., Brodribb, T.J., 2016. Linking Turgor with ABA Biosynthesis: Implications for stomatal responses to vapor pressure deficit across land plants. Plant Physiol. 171, 2008–2016. https://doi.org/10.1104/pp.16.00380

McDowell, N.G., Allen, C.D., 2015. Darcy's law predicts widespread forest mortality under climate warming. Nat. Clim. Chang. 5 (7), 669–672. https://doi.org/10.1038/nclimate2641

Mediavilla, S., Escudero, A., 2003. Stomatal responses to drought at a Mediterranean site: a comparative study of co-occurring woody species differing in leaf longevity. Tree Physiol. 23, 987–996. https://doi: 10.1093/treephys/23.14.987.

Mediavilla, S., Escudero, A., 2004. Stomatal responses to drought of mature trees and seedlings of two co-occurring Mediterranean oaks. For. Ecol. Manag. 187, 281–294. https://doi:10.1016/j.foreco.2003.07.006

Miller, D.P., Howell, G.S., Flore, J.A. 1996. A whole-plant, open, gas-exchange system for measuring net photosynthesis of potted woody plants. Hortoscience 31, 944–946. https://doi:10.21273/HORTSCI.31.6.944

Moyan, L., Junqiang, Y., Jingyun, G., Jianghua, Z., 2021. Observed changes in vapor pressure deficit suggest a systematic drying of the atmosphere in Xinjiang of China. Atmos. Res. 248, 105199. https://doi.org/10.1016/j.atmosres.2020.105199

Novick K.A., Miniat, C.F., Vose, J.M. 2016. Drought limitations to leaf-level gas exchange: results from a model linking stomatal optimization and cohesion–tension theory. Plant Cell Environ. 39, 583–596. https://doi.org/10.1111/pce.12657

Novick K.A., Konings, A.G., Gentine, P. Beyond soil water potential: An expanded view on isohydricity including land–atmosphere interactions and phenology. 2019. Plant Cell Environ. 42, 1802–1815. https://doi.org/10.1111/pce.13517

Peguero-Pina, J.J., Sancho-Knapik, D., Barrón, E., Camarero, J.J., Vilagrosa, A., Gil-Pelegrín, E. 2014. Morphological and physiological divergences within *Quercus ilex* support the existence of different ecotypes depending on climatic dryness. Ann. Bot. 114(2), 301-13. https://doi.org/10.1093/aob/mcu108.

Peguero-Pina, J.J., Mendoza-Herrer, O., Gil-Pelegrín, E. Sancho-Knapik., D. Cavitation limits the recovery of gas exchange after severe drought stress in holm oak (*Quercus ilex* L.). Forests 9, 443. https://doi.org/10.3390/f9070443

Peguero-Pina, J.J., Vilagrosa, A., Alonso-Forn, D., Ferrio, J.P., Sancho-Knapik, D., Gil-Pelegrín, E., 2020. Living in drylands: functional adaptations of trees and shrubs to cope with high temperatures and water scarcity. Forests 11, 1028. https://doi.org/10.3390/f11101028

Postl, W.F., Bolhàr-Nordenkampf, H.R., 1983. 'GASEX': a program to study the influence of data variations on calculated rates of photosynthesis and transpiration. In Photosynthesis and production in a changing environment; Hall, D.O., Scurlock, J.M.D., Bolhàr- Nordenkampf, H.R., Leegood, R. C., Long, S. P., Eds.; Chapman and Hall: London, 1983; pp. 448-455

Restaino, C.M., Peterson, D.L., Littell, J., 2016. Increased water deficit decreases Douglas fir growth throughout western US forests. Proc. Natl. Acad. Sci. U. S. A. 113, 9557–9562. https://doi.org/10.1073/pnas.1602384113

Rey-Sánchez, A.C., Slot, M., Posada, J.M., Kitajima, K., 2016. Spatial and seasonal variation in leaf temperature within the canopy of a tropical forest. Clim. Res. 2016, 71, 75-89. https://doi.org/10.3354/cr01427

Ritz, C., Baty, F., Streibig, J. C., Gerhard, D., 2015. Dose-Response Analysis Using R. Plos One, 10(12), e0146021. https://doi.org/10.1371/journal.pone.0146021

Rosseel, Y. 2012. Lavaan: An R Package for Structural Equation Modeling. Journal of Statistical Software, 48(2), 1-36. URL http://www.jstatsoft.org/v48/i02/

Sancho-Knapik, D., Álvarez-Arenas, T.G., Peguero-Pina, J.J., Gil-Pelegrín, E., 2010. Air-coupled broadband ultrasonic spectroscopy as a new non-invasive and non-contact method for the determination of leaf water status. J. Exp. Bot. 61(5), 1385-1391. https://doi.org/10.1093/jxb/erq001

Sancho-Knapik, D., Medrano, H., Peguero-Pina, J.J., Mencuccini, M., Fariñas, M.D., Álvarez-Arenas, T.G., Gil-Pelegrín, E., 2016. The application of leaf ultrasonic resonance to *Vitis vinifera* L. suggests the existence of a diurnal osmotic adjustment subjected to photosynthesis. Front. Plant Sci. 7, 1601. https://doi.org/10.3389/fpls.2016.01601

Sancho-Knapik, D., Mendoza-Herrer, Ó., Gil-Pelegrín, E., Peguero-Pina, J.J., 2018. Chl fluorescence parameters and leaf reflectance indices allow monitoring changes in the physiological status of *Quercus ilex* L. under progressive water deficit. Forests 9, 400. https://doi.org/10.3390/f9070400doi:10.3390/f9070400

Seager, R., Hooks, A., Williams, A.P., Cook, B., Nakamura, J., Henderson, N., 2015. Climatology, variability, and trends in the U.S. vapor pressure deficit, an important fire-related meteorological quantity. J. Appl. Meteorol. Climatol. 54 (6), 1121–1141. https://doi.org/10.1175/JAMC-D-14-0321.1

Sepulcre-Canto, G., Zarco-Tejada, P.J., Jimenez-Munoz, J.C., Sobrino, J.A., Soriano, M.A., Fereres, E., Vega, V., Pastor, M., 2007. Monitoring yield and fruit quality parameters in open-canopy tree crops under water stress. Implications for ASTER. Remote Sens. Environ. 107, 455–470. https://doi.org/10.1016/j.rse.2006.09.014

Tatarinov, F., Rotenberg, E., Maseyk, K., Ogée, J., Klein, T., Dan Yakir, D. 2016. Resilience to seasonal heat wave episodes in a Mediterranean pine forest. New Phytol. 210, 485-496. https://doi.org/10.1111/nph.13791

Taylor, N.J., Smit, T.G., Midgley, S.J.E., Annandale, J.G. 2020. Stomatal regulation of transpiration and photosynthesis in macadamias. Acta Hortic. 1281, 463-469. https://doi.org/10.17660/ActaHortic.2020.1281.61

Tenhunen, A.J.D., Lange, O.L., Braun, M. 1981. Midday stomatal closure in Mediterranean type sclerophylls under simulated habitat conditions in an environmental chamber: II. Effect of the complex of leaf temperature and air humidity on gas exchange of *Arbutus unedo* and *Quercus ilex*. Oecologia 50, 5-11. https://doi.org/10.1007/BF00378788

Tenhunen, A.J.D., Serra, A.S., Harley, P.C., Dougherty, R.L., Tenhunen, J.D., Serra, A.S., Harley, P.C., Dougherty, R.L., Reynolds, J.F. 1990. Factors influencing carbon fixation and water use by Mediterranean sclerophyll shrubs during summer drought. Oecologia 82, 381-393. https://doi.org/10.1007/BF00317487

Tognetti, R., Longobucco, A., Miglietta, F., Raschi, A., 1998. Transpiration and stomatal behavior of *Quercus ilex* plants during the summer in a Mediterranean carbon dioxide spring. Plant Cell Environ. 21, 613–622. https://doi.org/10.1046/j.1365-3040.1998.00301.x doi.org/10.1046/j.1365-3040.1998.00301.xTurner, N.C., 1988.

Measurement of plant water status by pressure chamber technique. Irrigation Sci. 1988, 9, 289-308. https://doi.org/10.1007/BF00296704

Vilagrosa, A., Bellot, J., Vallejo, V.R., Gil-Pelegríin, E., 2003. Cavitation, stomatal conductance, and leaf dieback in seedlings of two co-occurring Mediterranean shrubs during an intense drought. J. Exp. Bot. 54(390), 2015-2024. https://doi.org/10.1093/jxb/erg221

von Caemmerer, S., Farquhar, G.D., 1981. Some relationships between the biochemistry of photosynthesis and the gas exchange of leaves. Planta 1981, 153, 376–387. https://doi.org/10.1007/BF0038425710.1007/BF00384257.

Williams, A.P., Allen, C.D., Macalady, A.K., Griffin, D., Woodhouse, C.A., Meko, D.M., Swetnam, T.W., Rauscher, S.A., Seager, R., Grissino-Mayer, H.D., Dean, J.S., Cook, E.R., Gangodagamage, C., Cai, M., McDowell, N.G., 2013. Temperature as a potent driver of regional forest drought stress and tree mortality. Nat. Clim. Chang. 3, 292–297. https://doi.org/10.1038/nclimate1693

Williams, A.P., Seager, R., Berkelhammer, M., Macalady, A. K., Crimmins, M. A., Swetnam, T. W., Trugman, A. T., Buenning, N., Hryniw, N., McDowell, N. G., Noone, D., Mora, C. I., Rahn, T. 2014. Causes and implications of extreme atmospheric moisture demand during the record-breaking 2011 wild fire season in the southwestern United States. J. Appl. Meteorol. Climatol. 53 (12), 2671–2684. https://doi.org/10.1175/JAMC-D-14-0053.1

Yuan, W., Zheng, Y.I., Piao, S., Ciais, P., Lombardozzi, D., Wang, Y., Ryu, Y., Chen, G., Dong, W., Hu, Z., Jain, A.K., Jiang, C., Kato, E., Li, S., Lienert, S., Liu, S., Nabel, J.E.M.S., Qin, Z., Quine, T., Yang, S. 2019. Increased atmospheric vapor pressure deficit reduces global vegetation growth. Sci. Adv. 5(8), eaax1396. https://doi.org/10.1126/sciadv.aax1396https://doi.org/10.1126/sciadv.aax1396

Draft pre-print version. *The final version of this article can be found at:*
Sancho-Knapik D, Mendoza-Herrer O, Alonso-Forn D, *et al*. 2022 Vapor pressure deficit constrains transpiration and photosynthesis in holm oak: A comparison of three methods during summer drought. *Agric. For. Meteorol.* 327, 109218. https://doi.org/10.1016/j.agrformet.2022.109218

Suplementary material

Table S1 Comparison of the temperature (*T*, °C) and vapor pressure deficit (VPD, kPa) conditions between the outside of the chamber (out) and inside the chamber (inside), showing the effects of Teflon FEP throughout the daytime in our experiment.

Solar time	*T* out	*T* inside	VPD out	VPD inside
6:00-7:00	18.6±0.5ª	17.5±0.5b	0.4±0.1ª	0.2±0.0b
8:00-9:00	25.2±0.4ª	25.7±0.2ª	1.4±0.1ª	1.4±0.0a
10:00-12:00	28.9±0.7ª	33.9±0.5b	2.1±0.1ª	3.3±0.1b
13:00-15:00	33.4±0.6ª	40.1±0.8b	3.6±0.2ª	5.5±0.4b
16:00-18:00	28.3±0.7ª	34.1±1.1b	2.2±0.2ª	3.2±0.3b

Data are mean ± se. Different letters indicates significant differences between the outside and inside the chamber (Student's t-test, $P<0.05$).

Draft pre-print version. *The final version of this article can be found at:*
Sancho-Knapik D, Mendoza-Herrer O, Alonso-Forn D, *et al*. 2022 Vapor pressure deficit constrains transpiration and photosynthesis in holm oak: A comparison of three methods during summer drought. *Agric. For. Meteorol.* 327, 109218. https://doi.org/10.1016/j.agrformet.2022.109218

Table S2 Analysis of variance (ANOVA) to assess the effects of measurement technique (METHOD: leaf cuvette, plant chamber, IR thermometry), soil water deficit (WATER: well watered / dry) and log-transformed values of vapor pressure deficit (logVPD) on standardized conductance. In bold *P*-values < 0.05.

	Df	Sum Sq	Mean Sq	*F* value	*P* value
METHOD	2	0.477	0.238	13.6	**<0.001**
WATER	1	12.397	12.397	706.3	**<0.001**
logVPD	1	84.173	84.173	4795.5	**<0.001**
METHOD:WATER	2	0.211	0.105	6.0	**0.002**
METHOD:logVPD	2	0.662	0.331	18.9	**<0.001**
WATER:logVPD	1	0.087	0.087	4.9	**0.026**
METHOD:WATER:logVPD	2	0.793	0.396	22.6	**<0.001**
Residuals	4073	71.492	0.018		

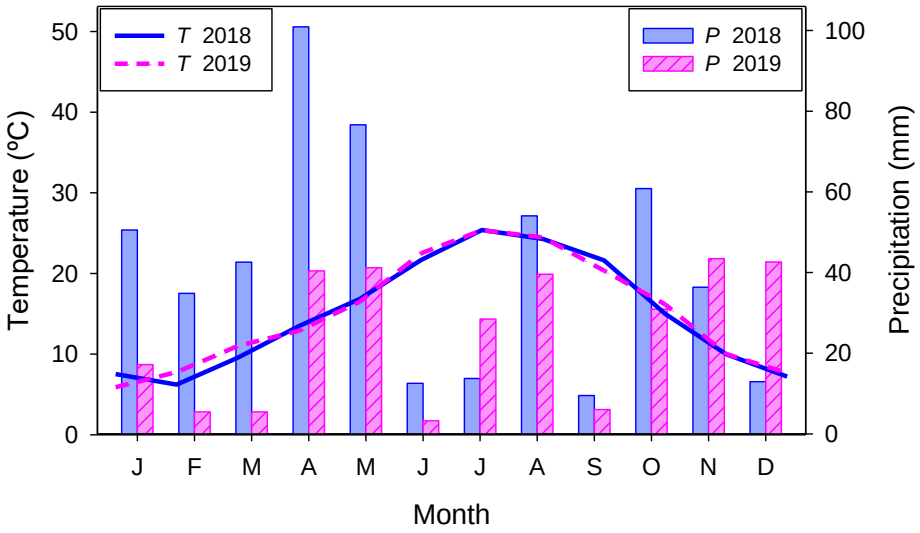

Fig. S1 Annual climate patterns in 2018 and 2019 of the study area. *T*, temperature; *P*, precipitation. Data obtained from the closest climatic station (41.722° N, 0.812° W, Zaragoza, Spain).

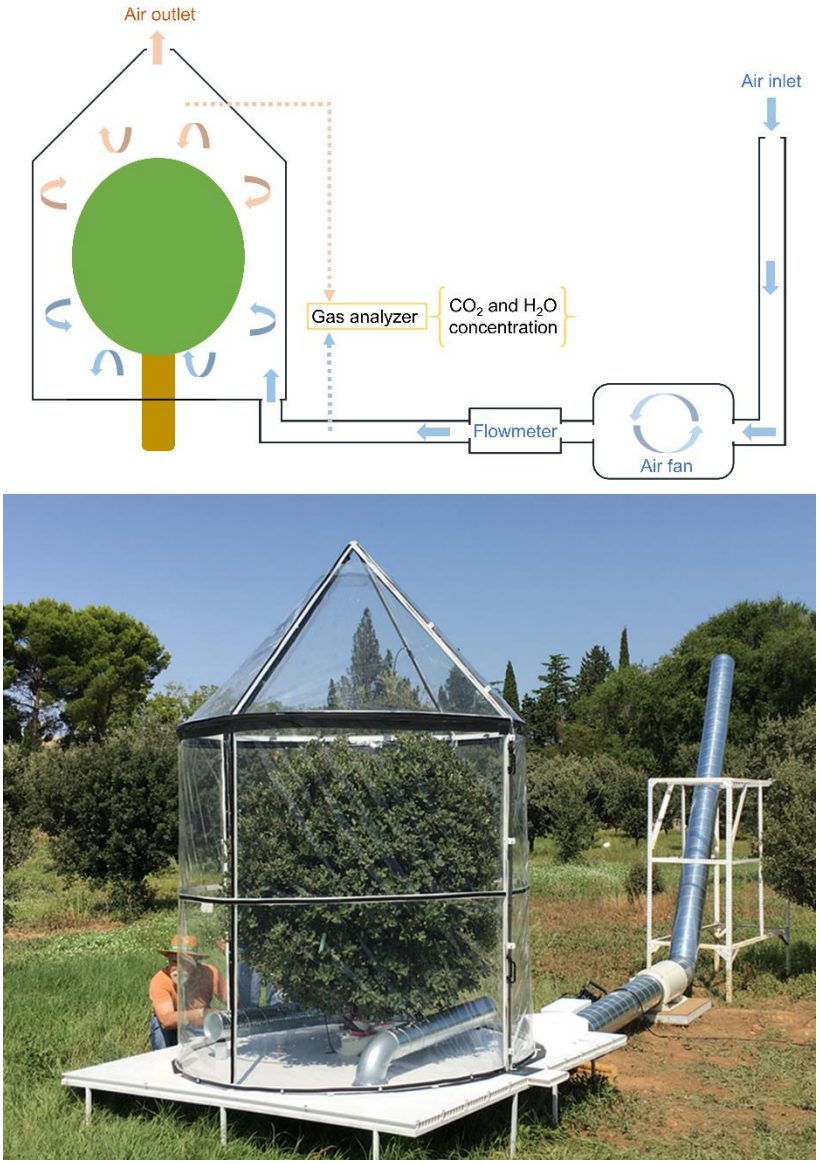

Fig. S2 Schematic representation and an image detail of the whole-plant chamber device used in this study.

Draft pre-print version. *The final version of this article can be found at:*
Sancho-Knapik D, Mendoza-Herrer O, Alonso-Forn D, *et al*. 2022 Vapor pressure deficit constrains transpiration and photosynthesis in holm oak: A comparison of three methods during summer drought. *Agric. For. Meteorol.* 327, 109218. https://doi.org/10.1016/j.agrformet.2022.109218

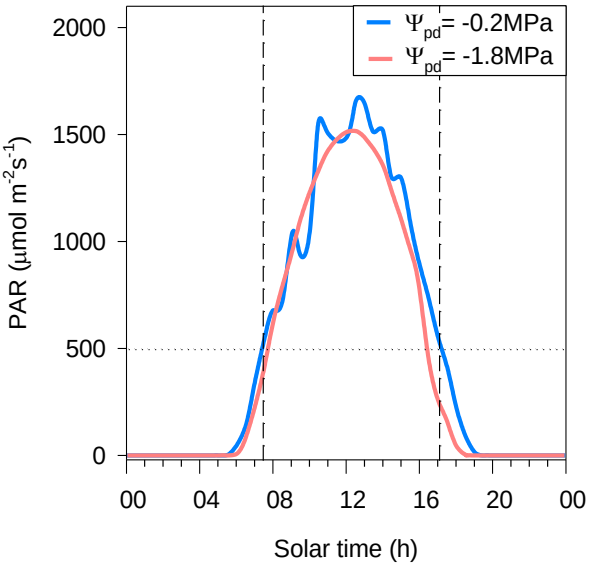

Fig. S3 Evolution of the photosynthetic active radiation (PAR) throughout the day monitored for one holm oak under well-watered conditions (blue; predawn water potential, Ψ_{pd}=-0.2 MPa) and on other specimen under drought conditions (red; Ψ_{pd}=-1.8 MPa), corresponding to the plot shown in Fig. 5a. Dashed lines define the time interval with a PAR higher than 500 µmol m^{-2} s^{-1}.

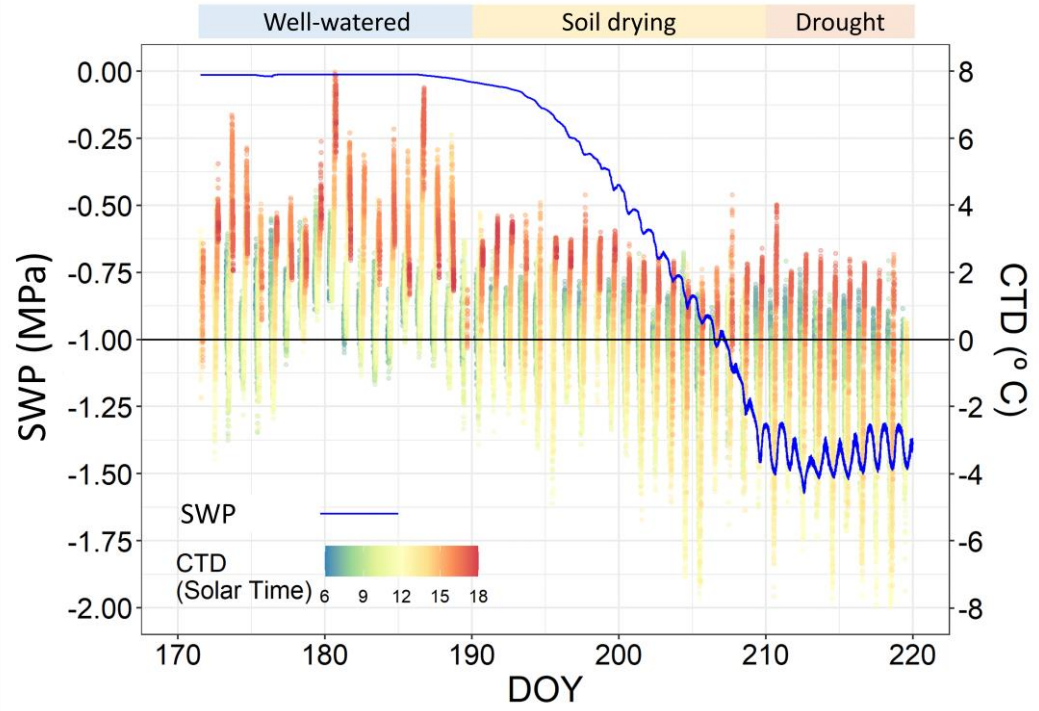

Fig. S4 Example of the evolution of the soil water potential (SWP) and the canopy temperature depression (CTD), measured on one holm oaks throughout a Mediterranean summer. DOY, day of year. Different colors in CTD indicates the solar time of the day, from 6:00 to 18:00 h. As a reference, the three main phases in the evolution of SWP are indicated.

Draft pre-print version. *The final version of this article can be found at:*
Sancho-Knapik D, Mendoza-Herrer O, Alonso-Forn D, *et al*. 2022 Vapor pressure deficit constrains transpiration and photosynthesis in holm oak: A comparison of three methods during summer drought. *Agric. For. Meteorol.* 327, 109218. https://doi.org/10.1016/j.agrformet.2022.109218

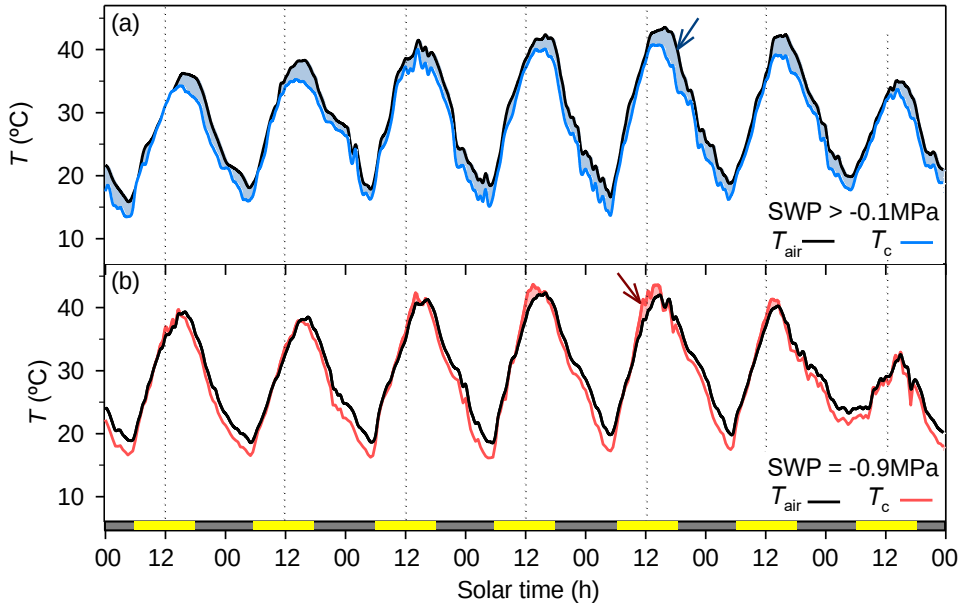

Fig. S5 Air (T_{air}) and canopy (T_c) temperatures monitored on one specimen of *Quercus ilex* subsp. *rotundifolia* using the infrared thermometry method. (a) corresponds to a 7-day period (day of the year 176 to 182) under well-watered conditions (soil water potential, SWP>-0.1 MPa) and (b) corresponds to a 7-day period (day of the year 201 to 207) under soil water deficit conditions (SWP=-0.9 MPa). Yellow and grey bars on the x-axis correspond to periods with a photosynthetic active radiation higher and lower than 500 µmol m^{-2} s^{-1}, respectively. The blue arrow in (a) indicates a moment where T_c is lower than T_{air}. The red arrow in (b) indicates a moment where T_c is higher than T_{air}.

Draft pre-print version. *The final version of this article can be found at:*
Sancho-Knapik D, Mendoza-Herrer O, Alonso-Forn D, *et al*. 2022 Vapor pressure deficit constrains transpiration and photosynthesis in holm oak: A comparison of three methods during summer drought. *Agric. For. Meteorol.* 327, 109218. https://doi.org/10.1016/j.agrformet.2022.109218

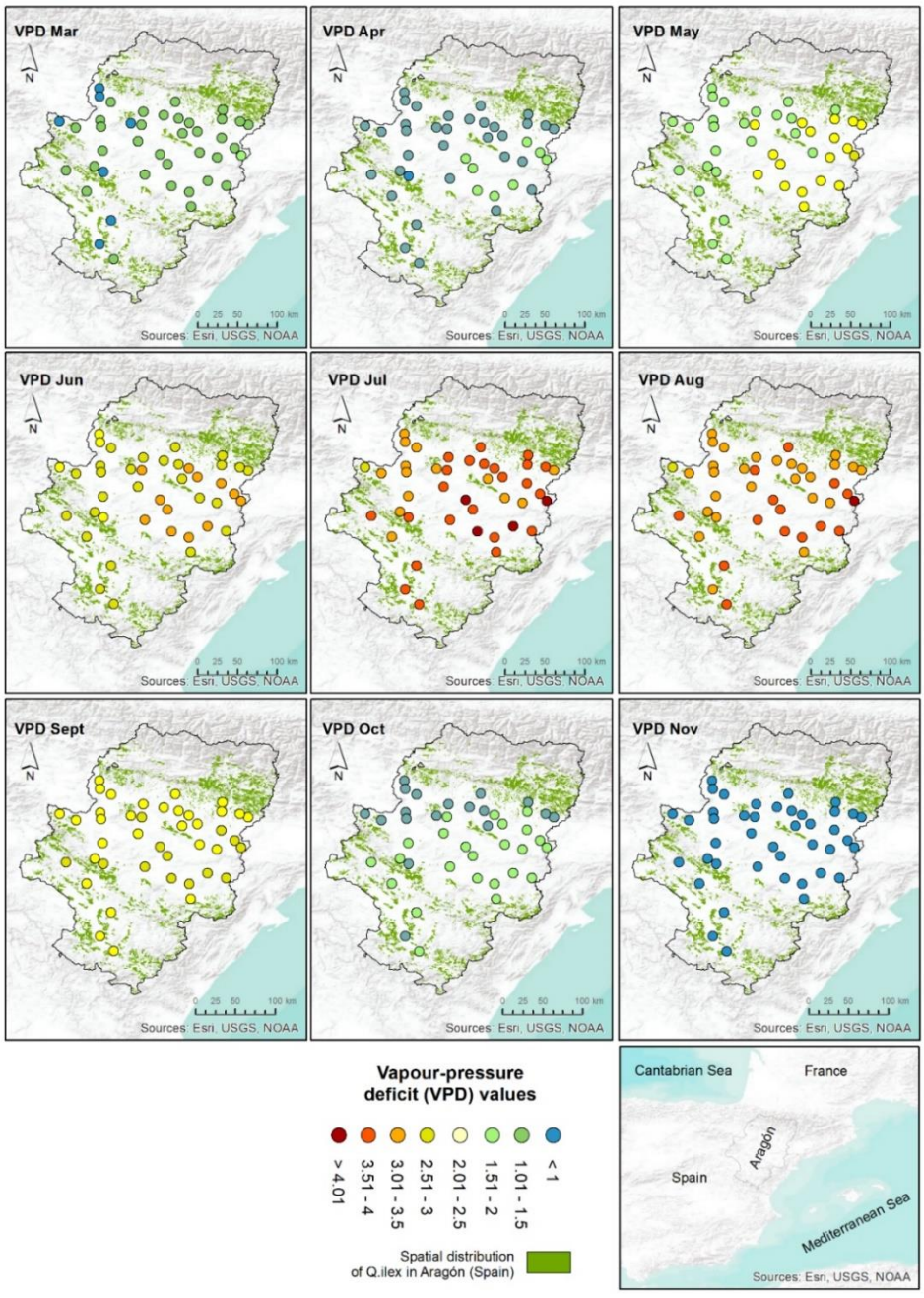

Fig. S6 Overlay map of the natural spatial distribution of *Quercus ilex* subsp. *rotundifolia* (shaded green) and VPD range values through the vegetative period, from March to November (colored circles) in Aragón (Northeast of Spain). Each circle corresponds to a meteorological station. VPD was calculated as the mean monthly value of a 10-year-period, from 2010 to 2020. Climatic data obtained from SIAR-Sistema de Información Agroclimática para el regadío www.siar.es (Ministerio de Agricultura y Pesca, Alimentación y Medio Ambiente).